Hydrophobic phytic acid conversion layers for corrosion protection of steel surfaces

Michelle Weinert, Jochen S. Gutmann, Michael Dornbusch

Abstract The possibility for a good conversion protection based on phytic acid (PA) solutions is described many times in the literature.[1,2] The latest results show that PA cannot improve the corrosion protective properties with an organic coating,[2] although PA conversion layers without organic coatings have already successfully been applied on different surfaces and the development of layers with enhanced corrosion protective behavior was possible.[3,4] The reason why PA does not work together with an organic coating is based on the hydrophilic surface and therefore the low contact angle of the PA conversion layer.[2] One solution is to modify PA directly and/or change the solution properties to increase the hydrophobic properties. In this work, a new and innovative way to synthesize a new type of sustainable organic PA-based conversion layers on steel, which works completely without titanium or zirconium and is a new approach for hydrophobic conversion layers, is presented.[5] The results prove the formation of a pure PA-based conversion layer on the surface. The infrared (IR), Raman, and nuclear magnetic resonance (NMR) spectroscopy verified the new synthesis products and by means of the vibration spectroscopy, the resulting conversion layers. To analyze the new physical properties, the contact angle of the conversion layers was detected. By means of the electrochemical impedance spectroscopy (EIS), the electrochemical stability of the conversion was studied and with cyclic voltammetry (CV), the solidity ratio was investigated. At last, the corrosion protective performance of the layers in combination with an E-coat in the salt spray test (SST) was examined. All modified PA-based conversion layers in combination with E-coats increased the corrosion protective properties in relation to industrial used phosphate conversion layers of steel surfaces. The overall result is a new kind of hydrophobic phytic acid-based conversion layer which shows advanced anticorrosion and coatability properties compared to other layers based on PA. The results if the EIS measurements show that the resistance of the coating significantly increased, and diffusion could be suppressed by coating the metal surface with PA conversion layers. The comparison of the SST results for the reference and the modified PA underline these observations. The overall SST rating increased by 2 and the delamination went down to 1.9 mm while the corrosion was 0.1, comparable to phosphated steel.

Keywords Phytic acid, Conversion layer, Corrosion protection, E-coat, Esterificartion of phyrtic acid

M. Weinert, M. Dornbusch (✉)
Department of Chemistry and Institute for Coating and Surface Technology ILOC, Niederrhein University of Applied Sciences, Adlerstr. 1, 47798 Krefeld, Germany
e-mail: michael.dornbusch@hs-niederrhein.de

M. Weinert, J. S. Gutmann
Department of Chemistry, Physical Chemistry and CENIDE, University of Duisburg-Essen, Universitätsstr. 2, 45141 Essen, Germany
e-mail: jochen.gutmann@uni-due.de

Introduction

A big field of interest in applied research is the development of innovative and green corrosion protective coatings. Green corrosion protection will be a major industrial topic in the future due to the fact that conventional corrosion protection comes along with many downsides. The production of metallic coating steels is a highly energy intensive and therefore CO_2 emitting process. The annual damage by corrosion adds up to $276 billion, or 3.1% of the US's GDP.[6] Modern anticorrosion systems often consist of two layers. The first layer is an inorganic based conversion layer and the second layer an organic coating, often E-

coat systems. The conversion layers are deposited by autophoretic processes and in particular phosphate coatings are used.[7,8] The current problem is not the corrosion properties of the phosphate coatings but the use of phosphorous resources and the harmful characteristics of conventional conversion layers to humans and the environment, due to their sometimes-carcinogenic properties (e.g., nickel cations) and finally the resulting waste.[9] There are many different approaches for innovative corrosion protection systems and one "green" alternative could be phytic acid. The literature described this many times.[2–5]

Different ways to achieve PA conversion layers for a broad bandwidth of substrates like magnesium alloys[10–11] and steel surfaces[3,12] have been described in the literature. Most of these concepts focus on varying the ingredients of the dip bath solutions to form complexes and gain better conversion layers for example with metal oxides,[12] silanes,[13] molybdate[14], or iodide additives[4] but no concepts for chemically modified PA as a corrosion inhibitor were introduced especially on steel up until now. The main problem is that PA layers are unsuitable with organic coatings. Reasons were also described. One presumption is the high hydrophilic behavior of the PA conversion layers.[2] This behavior is a result of the terminal phosphate groups of the PA.

Two strategies to reach the goal of a "green" and usable conversion layer were introduced:

1. Generating a hydrophobic surface through modification of the PA
2. Changing the solution components (adding molybdate or oxides)

The modification of the PA was achieved through the conversion of PA with alcohols which resulted in new products with covalent bonds between the PA and the alcohols for the first time. The modification is meant to reduce the hydrophilic properties of PA to produce a hydrophobic PA layer on the surface.

Additionally, the bath composition was varied as described in the literature to further increase the corrosion protective behavior of the PA conversion layers. Proven methods like the addition of molybdate (a nontoxic inhibitor for better corrosion properties[2,14] and metal oxides [as a crosslinker for the PA molecules[12,15, 16])] in combination with the modified PA were used to optimize the performance. Metal oxides should increase the number of saturated P-OH groups in the coating and increase the hydrophobicity and the crosslinking of the phytic acid in the coating.

With these concepts, the goal of a sustainable conversion layer based on phytic acid should be achieved which shows excellent corrosion protective behavior in combination with an industrially used E-coat. The corrosion protective mechanism and the structure of the conversion layer will be analyzed by spectroscopic and electrochemical methods and the corrosion protective performance by means of salt spray test.

Characterization and materials

Characterization

Contact angle/Surface Energy The contact angles of deionized water on the conversion layers were evaluated with a Data-physics Contact Angle System OCA 15 plus Device. Water and diiodomethane (Thermo Scientific, purity $\geq 0.17 em 99.9\%$)) were used for the surface energy estimation.

Acid numbers (AN) The acid numbers were determined according to DIN EN ISO 2114:2002.

Electrochemical impedance spectroscopy (EIS) The EIS spectra were performed with a Zahner Zennium, Zahner-Elektrik GmbH. The apparatus consisted of a 2-electrode setup and a solution of 3 wt% NaCl (Carl Roth, purity $\geq 99.8\%$) in deionized water was used as electrolyte. The amplitude was set to 10 mV. The frequency range was 100 mHz to 100 kHz. Stainless steel (steel number: 14565) served as counter electrode (CE) (Fig. 1).

Cyclovoltammetry (CV) The CV spectra were performed with a Zahner Zennium, Zahner-Elektrik GmbH in a 3-electrode setup. A solution of 3 wt% NaCl (Carl Roth, purity $\geq 99.8\%$) in deionized water was used as electrolyte. Stainless steel (steel number: 14565) served as counter electrode. E_{start} was -600 mV, E_{upper} was -300 mV, and E_{lower} was -1 V. The scan rate was 5 mV/s (samples) or 100 mV/s (noncoated steel). Reference electrode (RE) was Ag/AgCl.

Salt spray test (SST) The SSTs were performed in a Liebisch Laborgeräte; Constatwin device, according to DIN EN ISO 9227. Delamination tests were performed with duct tape rip off.
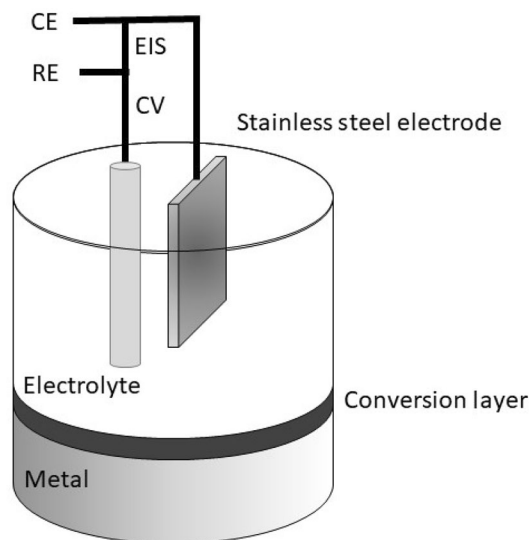

Fig. 1: Scheme of the electrochemical setup for the EIS (2-electrode setup) and the CV (3-electrode setup) measurements. The cell is a PVC-based pipe fixed on the covered metal sheet by pressure (see Fig. 1).

Crosscut Test The crosscut tests were performed in according to DIN EN ISO 2409.

IR The IR spectra were performed with an FTIR Lumos Microscope from Bruker at the ATR modus from 500 to 3900 cm^{-1} with a resolution from 4 cm^{-1}.

Raman The Raman spectra were performed with Cora5X00 from Anton-Paar with a 785 nm laser with a Raman shift from 0 to 2500 cm^{-1} with a resolution of 6 cm^{-1}.

Scanning Kelvin Probe (SKP) SKP was from Wicinski–Wicinski GbR and calibration was done using copper sulfate (1 mol/L).

Nuclear magnetic resonance (NMR) The Bruker DRX500 with 5 mm QNP sample head was used for $^1H, ^{13}C,$ and ^{31}P NMR measurements. For the data evaluation, the software TopSpin for Windows was used.

SEM The SEM-EDX spectra were performed with a Hitachi S-3400N. The accelerating voltage was set to 5 kV.

Pycnometer For a first estimation of the layer thickness, the weight difference before and after the coating process was measured with a scale with a resolution from 0.0001 g and the density was measured using the pycnometer. The densities were determined according to DIN 53217. The samples were cut off the surface using a cutting knife.

Thickness measurement Thickness measurements were performed with a Coatmaster 3D and an eddy current process (EN ISO 2808 process 7C) to validate the method. A MiniTest 4100 from Elektrophysik, a magnetic inductive device, was used for the measurement of the reference samples.

UV–VIS UV–VIS spectra were performed by Varian Cary 5000 UV–Vis–NIR spectrometer, and performance was measured in the 200–3300 nm range.

All experiments were measured at least three times to verify the results.

Materials and modified PA structures

Materials

PA with a concentration of 50 wt% in water was bought from Acros Organics. Toluene, ethanol, isopropanol, iron oxide, and ammonium hepta-molybdate from Carl Roth were used. Decanol, 10-undecen-1-ol, 2-phenyl-3-propanol, urea, dimethyl urea, and L-asparagine from VWR chemicals were used. The used potassium nitrate was bought from Sigma-Aldrich.

Substrates

DC04 steel from Chemetall Germany was used for the application of the conversion layers. Noncoated DC04 steel was used as negative reference and zinc phosphate steel was taken (DC04 + ZE) as state-of-the-art reference. To clean the metal surfaces, they were wiped with ethanol and then ultrasonically washed for 5 min in deionized water at room temperature. After that, they were wiped with isopropanol and ethanol again.

E-coat

Moreover, the CDP process was executed with products from Axalta, the pigment paste 8D55-02399 and the binder 8D55-02932.

Experimental methods

Synthesis

Synthesis of the PA-alcohol products

The principal synthesis of PA esters had already been shown in the literature. It was reported that PA molecules can successfully be converted with epoxides[17] while the esterification of PA with alcohols is a new and promising way to produce PA esters which has not been reported yet. The reaction was carried out at temperatures higher than 120 °C to gain higher yields and conversion rates. At these temperatures, PA tends to undergo autohydrolysis reactions while the successful formation of phosphate esters proven by AN data.[18,19] Due to this behavior, it is assumed that the resulting product is a higher mixture of phosphate esters of different myo-inositol phosphates, which originate from the described autohydrolysis, with the respective alcohols used for the different reactions.

Three different approaches were used to increase the hydrophobicity of the PA conversion layers and make it compatible with an industrial E-coat:

1. Increasing the hydrophobicity of PA through chemical modification (samples 1–5)
2. Further increasing the reactivity with an industrial E-coat through the addition of urea-PA reaction products (samples 6 and 7)
3. Trying to achieve amide formation through reaction with amine containing reaction partners (sample 8)

Synthesis with the right entrainer at the optimal conditions was successfully accomplished. Three variations with different turnover rates were synthesized from the reaction undecen-1-ol. Different amounts of reactive hydrogen groups of the PA were successfully converted with alcohols to achieve different hydrophobicities. The molar ratios between PA and the OH-

functional molecules were varied, so that a respective maximum of the total reactive hydrogen-atoms could be reacted, and the total amount of converted PA was measured by determining the acid number of the products. Moreover, undecen-1-ol with a terminal double bonds and 2-phenyl-3-propanol was used as an aromatic educt.

GENERAL PROCEDURE FOR THE ESTER FORMATION: First, 0.3 mol of a 50% phytic acid solution was evaporated at 70 °C, at 15 mbar for 5 h to increase the PA concentration to 84%. Then, 0.067 mol of phytic acid in 20 mL of toluene was weighed into a three-neck flask under nitrogen atmosphere and 0.397 mol (0.199 or 0.530 mol) of an

alcohol was added and heated up to 140 °C for 3–5 h, until no more reaction water accrued. Yield: 75 to 97%. The density is 2.3 g/cm^3.

From the new product with undecen-1-ol, three variations with different turnover rates were synthesized. Different amounts of reactive hydrogen groups of the PA were successfully converted with alcohols to achieve different hydrophobicities. The molar ratios between PA and the OH-functional molecules were varied, so that a respective maximum of the total reactive hydrogen atoms could be reacted, and the total amount of converted PA was measured by determining the acid number of the products. The reaction is assumed as shown in Fig. 2 (reaction scheme for one of the twelve phosphate groups). Table 1 shows the sample numbers from the experiments and Table 2 shows the reaction yields.
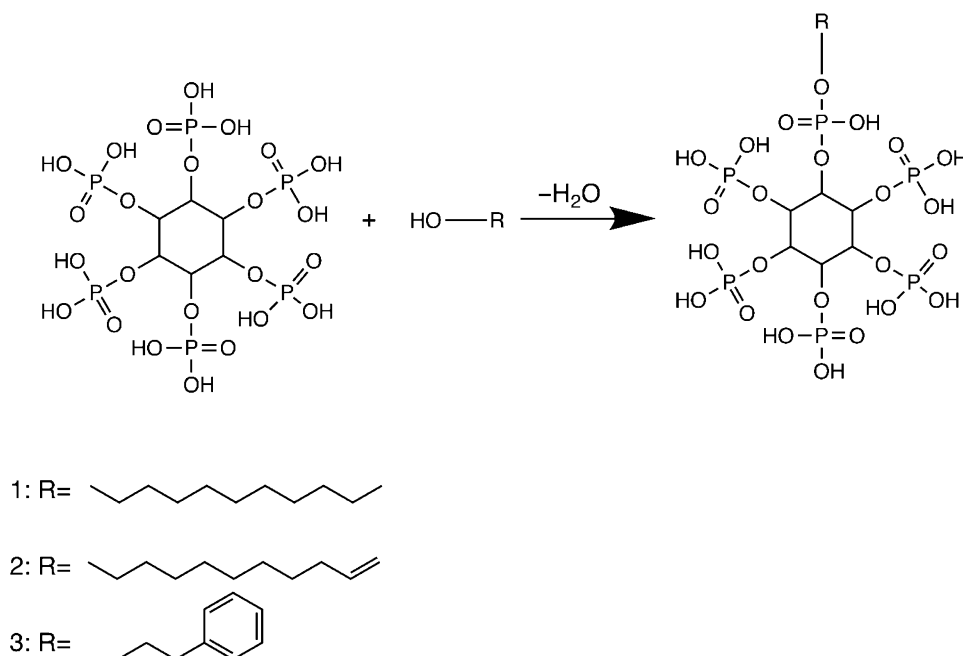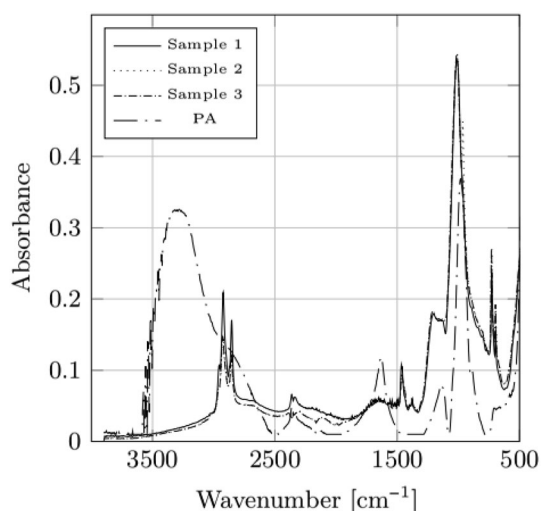

Fig. 2: Reaction of phytic acid with different alcohols

Table 1: Sample numbers from the experiments

Sample number	Molar ratio PA/Alc. or nitrogen compound	Theoretical molar mass [g/mol]	Theoretical sum formula
1	With six groups of decanol	1591.90	$C_{66}H_{138}O_{24}P_6$
2	With six groups of undecen-1-ol	1573.78	$C_{72}H_{138}O_{24}P_6$
3	With six groups of hydrolyzed 3-phenyl-1-propanol	1369.18	$C_{70}H_{78}O_{24}P_6$
4	With three groups of decanol	1125.93	$C_{36}H_{27}O_{24}P_6$
5	With eight groups of decanol	1902.52	$C_{86}H_{178}O_{24}P_6$
6	With six groups of urea	912.4	$C_{12}H_{40}N_{12}O_{24}P_6$
7	With six groups of dimethylurea (DMU)	1080.69	$C_{24}H_{54}N_{12}O_{24}P_6$
8	With six groups of L-asparagine	1344.76	$C_{30}H_{54}N_{12}O_{36}P_6$

Table 2: Yields of the products of reaction in Fig. 1

Sample number	Secluded water [mL]	Theoretically water [mL]	Yield based on secluded water [%]	Yield after recrystallization [%]
1	9.8	10.55	92.94	83.02
2	8.2	8.44	97.19	86.21
3	8.6	9.36	91.91	82.81
4	9	9.6	93.51	84.12
5	10	13.27	75.36	68.55

Fig. 3: IR spectra of PA products as liquid

To prepare samples for IR and NMR spectroscopy, all reaction products were first recrystallized in butanol (alcohol products) in terms of purification. The excess solvent was removed using a rotary evaporator afterward, and the samples were then dried in a vacuum oven over night.

Figure 3 shows the IR spectra from PA and the liquid products.

Figure 4 shows the IR spectra zoomed in at 4000 to 2500 cm^{-1} and Fig. 2 at 800 to 1200 cm^{-1}. Table 3 shows the resonance data of the relevant functional groups. PA has a significantly higher OH band than the reaction products. This can be related to the successful esterification. Moreover, a shift of the P–OH peak from 980 to 1010 cm^{-1} due to the reaction can be observed. The peak of the C=C double bond of sample 2 is clearly visible at 960 cm^{-1}.[8,20]

To determine the conversion rate, the acid numbers (ANs) were measured and compared to the theoretical AN for a complete conversion. Table 4 shows that the conversion rates reached the theoretical ANs in nearly all cases.

The results for the ANs show that the determined ANs are slightly higher than the theoretical ones.

These results occur due to the partial autohydrolysis of the PA during the synthesis process, the hydrolyzed PA shows a higher AN than pure PA. This behavior can also be observed for the products of converted groups based on the AN. For most of them, the AN is located between 5 and 6 groups. These results can be observed for all samples. In this case, the measured amounts of secluded water are approximately right. For sample 1 for example, the total number of converted groups based on the mass of secluded water is 5–6 groups. On the other hand, the number of converted groups based on the AN is also located between 5 and 6 groups.

Figure 5 shows the structure and the respective ^{1}H-NMR data of product sample 1 when only one alcohol is added. Figure 6 shows the ^{1}H-NMR spectrum of sample 1. The peak at 3.613 ppm splits as a triplet of doublet, because of the 2 H's of the other CH2 group (1) and the OH next to it. After the reaction, it can be observed that the triplet of doublet at 3.6 ppm transitioned into a triplet.

Coupling constants were estimated to verify the structure of the respective molecules. The measured values for the coupling constants for the peaks that changed during the reaction are 6.6 Hz and 7.0 Hz, as shown in Fig. 7. The difference between these values is about 5% which could be a result of the changing chemical surrounding and therefore changing angle between the respective atoms of the regarded group[22,23] (Fig. 7). Additionally, a characteristic peak for phytic acid appeared. On the other hand, the peak of the OH group at 1.84 ppm disappeared (see Fig. 6). Figure 7 shows the zoomed in peak at 3.5 ppm. The same behavior was observed for samples 2 and 3 as shown in Figs. 8 and 9.

The pure PA shows a peak at a shift of 4.8 ppm in the ^{1}H-NMR spectra, just like the reaction products (see "NMR spectra," Fig. 44). Furthermore, the ^{31}P-NMR data also proved the successful conversion during the reaction (see "NMR-spectra," Fig. 47). The pure PA shows a shift of approximately 0 ppm in the ^{31}P-NMR spectrum[24] while the reaction products show a higher shift to the upfield. This behavior can be observed due to the rising pH value of the solution;[25,26] the products show a pH value of 2–3 while pure PA dissolves with a pH of 1. Due to the pH-dependency,
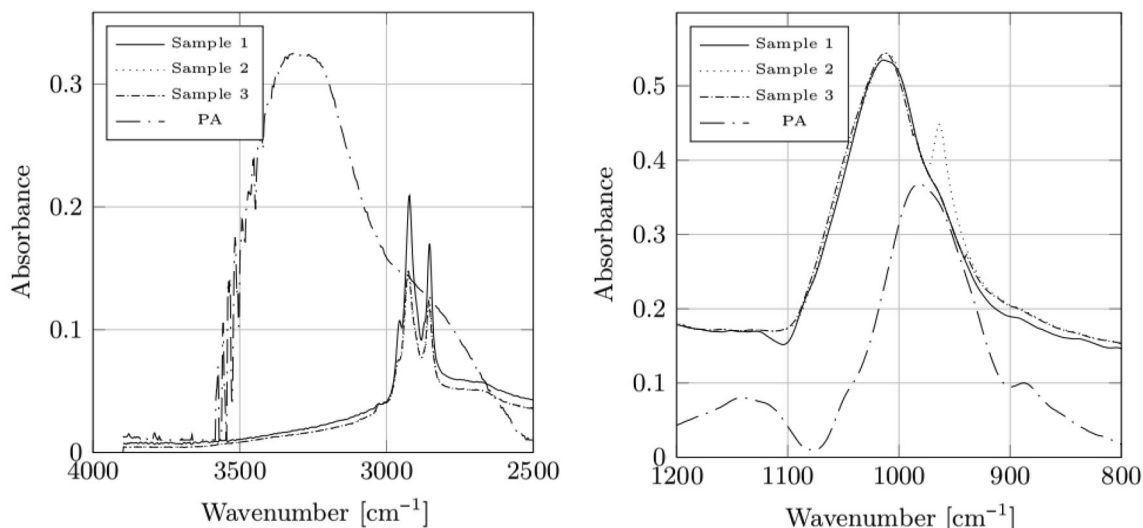
Fig. 4: IR spectra zoomed at 4000 to 2500 cm^{-1} and at 800 to 1200 cm^{-1}

Table 3: Important functional groups and respective resonance in [cm^{-1}] for the liquid products[8,20, 21]

Functional group	Resonance [cm^{-1}]
OH-valence	3223
Aryl-H-valence	3100
CH-valence	2914
CO_2	2350
–C–C– Skeletal vibrations	1615
OH deformation	1438
P=O and P=O–C stretch	1140
P–O– and P–O–C stretch	1000
C–H out-of-plane deformation vibration for C=C double bonds. (Only for sample 2)	960

Table 4: Theoretical and determined acid numbers.

Sample number	Theo. AN	Determined AN	In theo. converted acid groups	In determined converted acid groups	Molar mass based on AN [g/mol]
PA	1018.1	1077.0	0	0	660.04
1	509.1	542.14	6	$\sim$ 5–6	1431.58
2	509.1	515.8	6	$\sim$ 5–6	1497.64
3	509.1	512.3	6	$\sim$ 5–6	1310.09
4	763.6	817.5	3	$\sim$ 2–3	1010.74
5	339.4	423	8	$\sim$ 7	1642.00

the PA peak shifts. Moreover, the spectra of the reaction products show a second peak. This peak is further proof that a successful conversion took place because two different phosphate groups with one or two ester groups are observed in the product spectra.

The same could be identified for samples 2 and 3 (see ''NMR-spectra'').

Formation of the PA and nitrogen compounds products

Reactions of PA and nitrogen compounds (NCs) were performed. We proved that PA and small amounts of different NCs form stable salts, without further chemical reactions. Three different NCs were used and examined. The ratio between PA and the NC was

Sample 1:
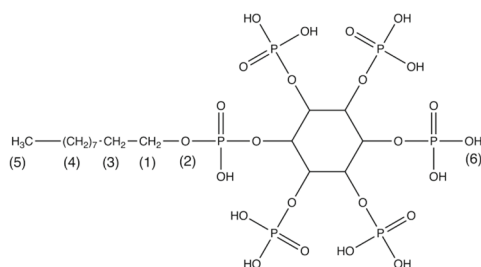
Group	^{1}H-NMR shift [ppm]	^{31}P-NMR shift (ppm)
CH of the inositol ring (6)	4.8 (singlet)	0.302
–CH_2– (1)	3.5 (triplet)	0.06
–CH_2– (3)	1.5 (multiplet)	
–$(CH_2)_7$(4)	1.3 (multiplet)	
–CH_3 (5)	0.9 (triplet)	

Fig. 5: Estimated structure of the product sample 1 and the respective ^{1}H-NMR peaks
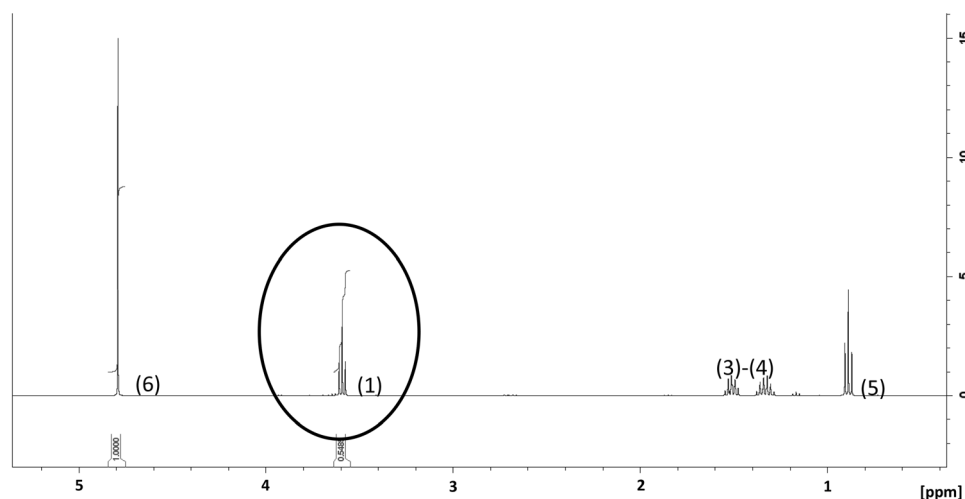
Fig. 6: NMR spectra of sample 1

chosen in a way that not all P–OH groups reacted with nitrogen groups, so that a part of the P–OH groups could graft toward the steel surface. In this case, all NCs showed the formation of the respective salts and not the assumed amide formation.

GENERAL PROCEDURE FOR THE SALT FORMATION: The same procedure was used for all NCs, because earlier experiments with L-asparagine proved the formation of ionic compounds (see Fig. 10).[27] Further experiments led to the conclusion that a simple mixture of PA and the respective NC showed the same results as the products of the previous reactions.

The molar ratios were picked the same way as for the alcohol experiments: first, 0.3 mol of PA was purified using a rotary evaporator, at 70 °C and 15 mbar for 5 h to increase the concentration of the PA to about 84%. Then, 0.067 mol of phytic acid and 0.402 mol of an NC were added to a reaction solution. The reaction was assumed as shown in Fig. 10. The figure shows an example for PA + urea (reaction scheme for one of the 12 phosphate groups). IR spectra of the products are illustrated in "Appendix spectra IR-measurements."

The –$NHCONH_2$ group of urea can be found at a Raman shift of 530 cm^{-1}.[8] The functional group of phytic acid is located at 910 cm^{-1}, while the –P–N–C–
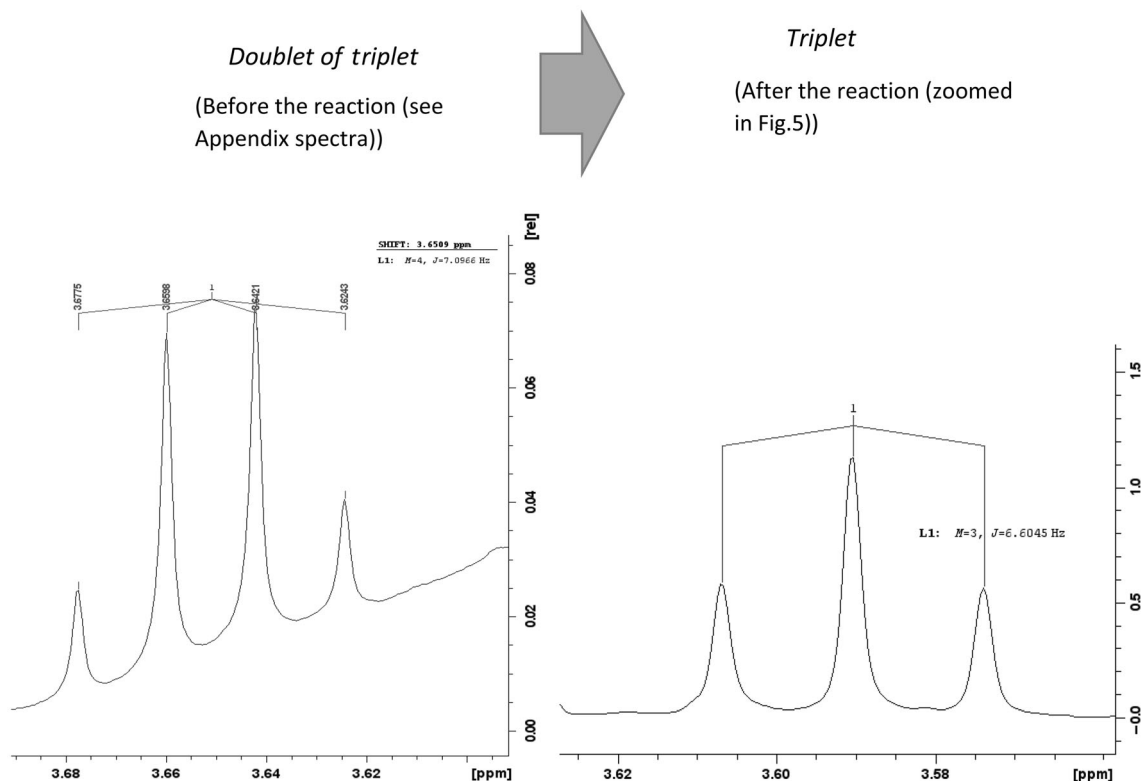
Fig. 7: Coupling constants for decanol and sample 1

Sample 2:
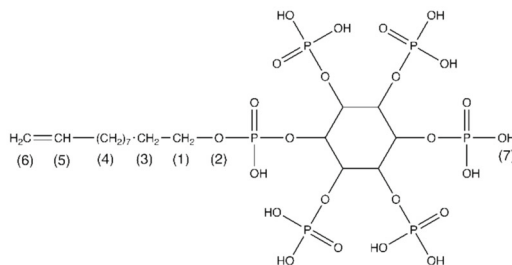
Group	^{1}H-NMR shift [ppm]	^{31}P-NMR shift (ppm)
CH of the inositol ring (7)	4.8 (singlet)	0.5
$-CH_2-$ (1)	3.5 (triplet)	0.04
$-CH_2-$ (3)	1.5 (multiplet)	$-$ 0.03
$-(CH_2)_7$ (4)	1.3 (multiplet)	
$-CH_3$ (5)	0.9 (triplet)	

Fig. 8: Estimated structure of the product sample 2 and the respective ^{1}H-NMR peaks

is at approximately 1000 cm^{-1}.[8] The –N–C–N– group of urea is visible at 1380 cm^{-1}.[8] The spectra confirm that phytic acid was successfully converted with urea.

The data show that after 2 h of reaction time significant changes in the peak intensities occur. After 4 h of reaction, the product changed from liquid to solid state

Sample 3:
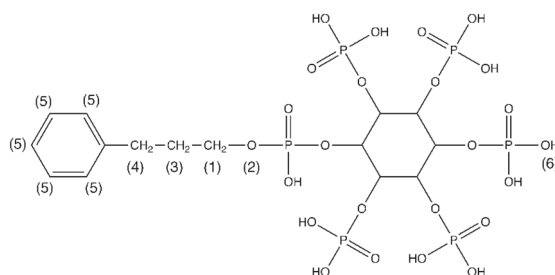
Group	^{1}H-NMR shift [ppm]	^{31}P-NMR shift (ppm)
CH of the inositol ring (6)	4.8 (singlet)	− 0.8
CH ring (5)	7 (multiplet)	− 1.03
(1)	3.6 (triplet)	− 1.33
(4)	2.7 (triplet)	− 1.56
(3)	1.8 (multiplet)	− 1.7
Leftover water	2.2 (singlet)	

Fig. 9: Estimated structure of the product sample 1 and the respective ^{1}H- and ^{31}P-NMR peaks
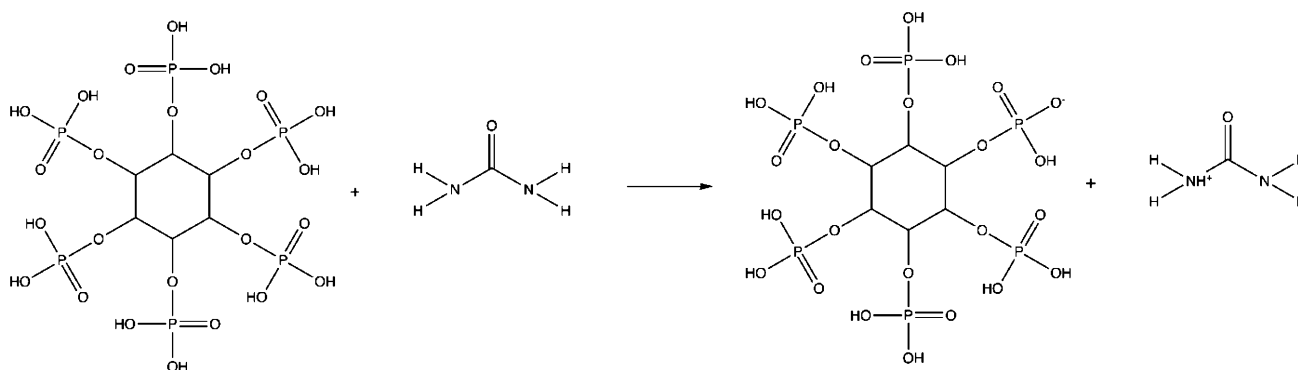
Fig. 10: Phytic acid and urea salt formation (sample 6)

of aggregation, so that no further Raman measurements were possible with this setup (see Fig. 11).

The wavenumbers at 421 cm^{-1} and 1300 cm^{-1} are an indicator for the –CO–NH–CH$_3$– of the DMU.[8] The hydroxy group of phytic acid, which loses intensity over time, can be observed at 904 cm^{-1} with ongoing reaction, and a peak at 1000 cm^{-1}[18] can be observed, which likely belongs to the developing ionic bond between the PO anions and urea cations. The wavenumbers 1156 cm^{-1} and 1187 cm^{-1} display the asymmetric –N–C–N– group.[8] The symmetric –N–C–

N– group can be found at 369 cm^{-1} and 1471 cm^{-1}.[8] The viscosity of the products increases over the reaction period, and this is the reason why the spectra, after a total reaction time 12 h, are less intense than the spectra after 4 h of reaction. The results of the Raman measurements underline the assumption that the conversion was successful (see Figs. 11, 12 and 13).

All in all, the Raman and NMR spectra (see Appendix for NMR "Appendix NMR spectra") also prove that formation of ionic compounds occurred. The Raman spectra show no significant difference
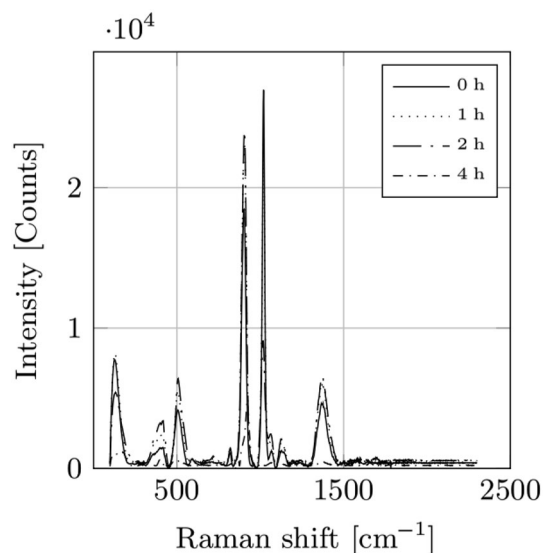
Fig. 11: Raman spectra of sample 6
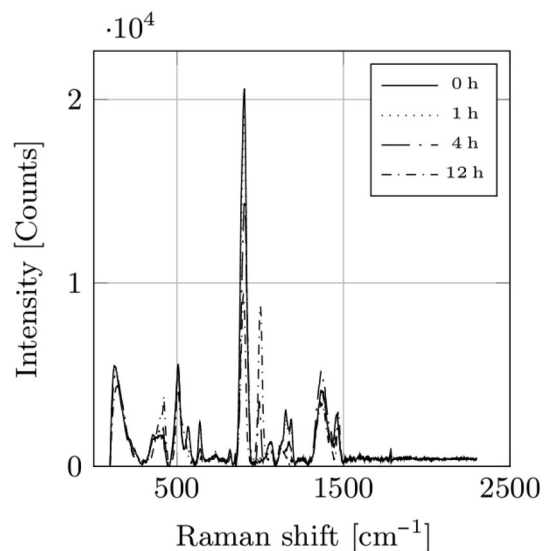
Fig. 12: Raman spectra of sample 7

between the educt and product spectra, what leads to the conclusion that no amide formation took place and thus the product bonds only show ionic character.

Formation of a conversion layer

Synthesis products conversion coatings

For these experiments, a PA solution, or one with the respective hydrophobic modification products, with a concentration of approximately 5 wt% in deionized
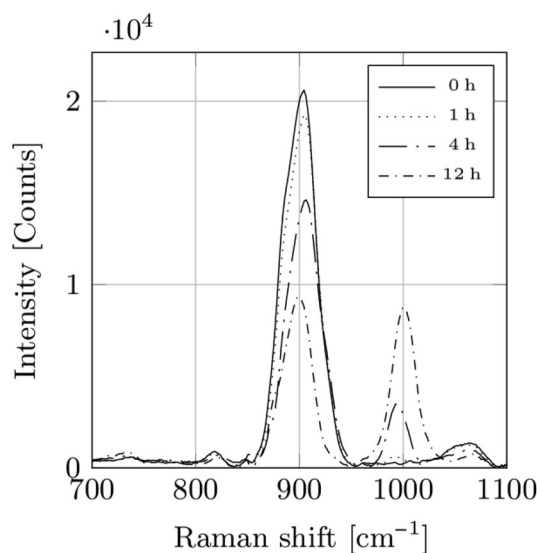

Fig. 13: Zoomed-in Raman spectra of sample 7

water was used. The optimal pH value is 2–3. The pH values lied within this range during all experiments, thus it was not needed to readjust the values later on. Other references stated before that PA can be used in broader pH spans.[28] Further experiments showed that an adjustment of the pH values had no significant influence compared to the conventional phosphating process, where the coating results are strongly dependent on the exact pH setting.[29] PA has 12 replaceable protons, whereby six are strongly acidic (pKa approximately 1.5), three are weaker acidic (pKa between 5.7 and 7.6), and three are very weak acidic (pKa > 10.0). Therefore, the buffering area is broader, and this behavior of PA is the main reason why the PA conversion technology is very resistant to pH value fluctuations.[30] Potassium nitrate was added as a promoting agent (2 g/L) and to reach better corrosion properties, the inhibitor ammonium hepta-molybdate (Mo, 10 wt%), which had already been studied in other publications, was used.[31,29] The temperature of the solution was set to 35 °C and the steel surfaces were dipped into the bath for 7 min. After that the surfaces were washed with water for final cleaning.

In another step, PA-NC salts and PA-alcohol esters were mixed and as another optimization step because it was expected that the addition of the PA-NC salts would further increase the compatibility of the conversion layers with the organic E-coat. Different metal oxides were added to the bath solutions. It was expected that a higher concentration of free metal ions in the bath solution would lead to a higher saturation of the PA molecules with metal ions that would directly increase the precipitation and density of the resulting conversion layers. For both optimization approaches, the total weight percentage of products in the solution was kept at 5 wt% while the ratio between the NC salts and the PA-alcohol esters was 1:1. For the

optimization step with iron oxide, 0.5 g/L iron(III) oxide was added to the sample. Figure 17 shows how the optimal amount of iron oxide was estimated (see below).

Formation of the conversion coatings

PA WITH UNDECANOL (SAMPLE 1, 4 AND 5): All compounds together result in a homogeneous mixture. The pH value of this mixture is between 1.7 and 2.7. The thickness of the conversion layers is 300 nm $\pm$ 80 nm with a density of 2.3 g/cm^3. The measurement was carried out through weighing the weight difference before and after the coating process. Therefore, the density of the surfaces had to be evaluated through scrapping of the conversion layer off the surface.

PA WITH UNDECEN-1-OL (SAMPLE 2): All compounds together result in a homogeneous mixture. The pH value of this mixture is 2.0. The thickness of the conversion layer is also at about 300 nm $\pm$ 80 nm with a density of 2.3 g/cm^3.

PA WITH 3-PHENYL-1-PROPANOL (SAMPLE 3): All compounds together result in a homogeneous mixture. The pH value of this mixture is 2.7. The thickness of the conversion layer is 240 nm $\pm$ 80 nm with a density of 2.3 g/cm^3.

Expected mechanism of the conversion layer formation

The film formation of the hydrophobic modified phytic acid should be based on an autophoretic process and the hypothesis for the film formation is described as follows:

During the dipping process, iron ions from the steel surface dissolve into the acidic solution as anodic reaction and the pH value of the solution increases due to the development of hydrogen as a product of the cathodic reaction (see Fig. 14a), i.e., an acidic corrosion mechanism.

The hydrogen evolution that increases the pH value near the surface caused the exceeding of the solubility product of iron phytate and molybdates precipitate on the surface. The molybdate should form bronzes with iron or salts. Because of the high functionality of the modified phytic acid, the formed layer is crosslinked during the precipitation (see Fig. 14b).

The resulting phytate complex conversion layer grants corrosion protection by a crosslinked layer and increased hydrophobicity. The overall result is a mix of two different layers[14] as described in literature which both increase the anticorrosion properties on the substrate surface (see Fig. 14c).

Conversion layers with cathodic dip coating

Two-layer system

A cathodic dip coating (E-coat) was from Axalta; 39.7% of the binder (8D55-02932) with 54.2% VE water and 6.1% pigment paste (8D55-02399) were used. The bath had a temperature of 35 °C and the surfaces were dipped for 150 s. After the dipping process, all samples were air-dried for approximately 5 min. Then, the coated surfaces cured in an oven at 180 °C for 15 min.

Because new conversion layers were used for the E-coat application, the deposition process had to be optimized. The most homogeneous surface was received at a voltage of 200 V and a dip time of 150 s. Settings between 180 and 400 V as well as different times from 60 to 200 s were also investigated. The application tests show that the best results were achieved when the samples were exposed to air for 5 min and afterward cured at 180 °C for 15 min. This procedure provides homogenous surfaces without any damages.

The thickness of these hydrophobic PA coatings with E-coat was around 23 to 25 μm. Figure 15 shows the calibration line with the respective regression function ($y = 0.0697x + 14.9$; $R^2 = 0.885$). The calibration was carried out regarding this data. In this case, 60 s stands for 60 s of application time.

Due to these results, all further samples were prepared under the aforementioned bath conditions as well as 200 V and 150–180 s of dipping time.

Results and discussion

Characterization of the conversion layer

Contact angle

To describe the hydrophobicity of the phytic acid-based conversion coatings in comparison with phosphate-based conversion coatings, contact angles against water and the surface energy by means of the Fokes Model[32] have been performed.

After the autophoretic process, the surfaces were cleaned in two steps, in the first step with deionized water, and in the second step with solvents, to guarantee that no unbounded alcohol was measured on the surface. After drying at room temperature, a contact angle measurement was carried out using 1 μL water or diiodomethane drops. Figure 16 shows the results of the contact angle measurements with water. Sample 1 reached a contact angle of 115°, which is comparable to the performance of the reference phosphate conversion layer, which also had a contact angle of 115°. The PA reference sample came out at 20°. Hence, the contact angle of the modified PA shows a significant improvement. The results show that a
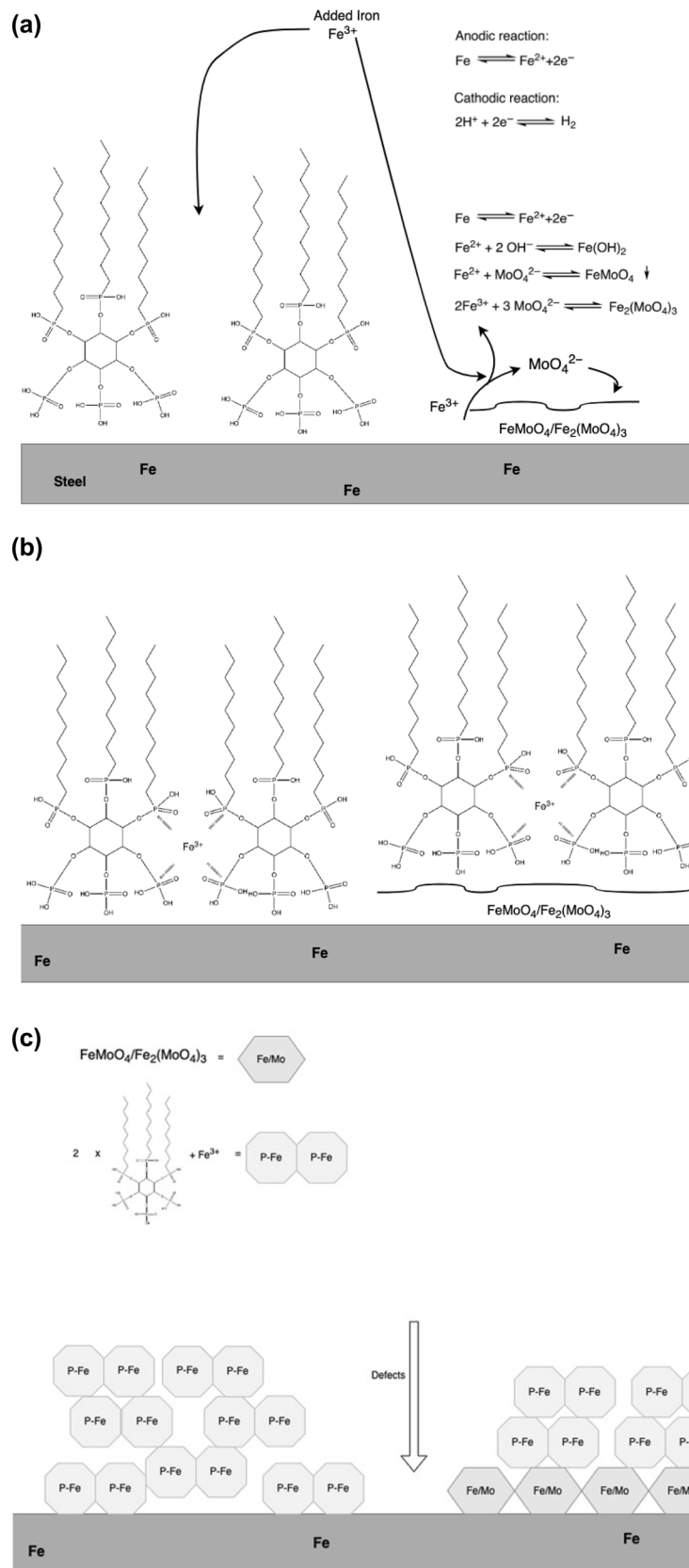
(a)

Added Iron
Fe^{3+}

Anodic reaction:

$Fe \rightleftharpoons Fe^{2+} + 2e^-$

Cathodic reaction:

$2H^+ + 2e^- \rightleftharpoons H_2$

$Fe \rightleftharpoons Fe^{2+} + 2e^-$

$Fe^{2+} + 2\,OH^- \rightleftharpoons Fe(OH)_2$

$Fe^{2+} + MoO_4^{2-} \rightleftharpoons FeMoO_4 \downarrow$

$2Fe^{3+} + 3\,MoO_4^{2-} \rightleftharpoons Fe_2(MoO_4)_3$

MoO_4^{2-}

Fe^{3+}

$FeMoO_4/Fe_2(MoO_4)_3$

Steel   Fe   Fe

Fe

(b)

Fe^{3+} Fe^{3+}

$FeMoO_4/Fe_2(MoO_4)_3$

Fe   Fe   Fe

(c)

$FeMoO_4/Fe_2(MoO_4)_3$ = Fe/Mo

$2 \times$ $+ Fe^{3+}$ =   P-Fe P-Fe

P-Fe P-Fe P-Fe P-Fe

Defects

P-Fe P-Fe P-Fe P-Fe

P-Fe P-Fe P-Fe P-Fe

P-Fe P-Fe P-Fe P-Fe

P-Fe P-Fe P-Fe P-Fe

Fe/Mo Fe/Mo Fe/Mo Fe/Mo

Fe   Fe   Fe

Fig. 14: Expected mechanism of the conversion layer formation (a), the molecular structure (b) and the microscopic structure (c)

successful modification of PA resulted in a conversion layer with strong hydrophobic properties.

All mixtures show high contact angles comparable to the alcohol products (see Table 5). This happens because the contact angle is a surface method, and the

Fig. 15: E-coat layer thickness measured with Coatmaster
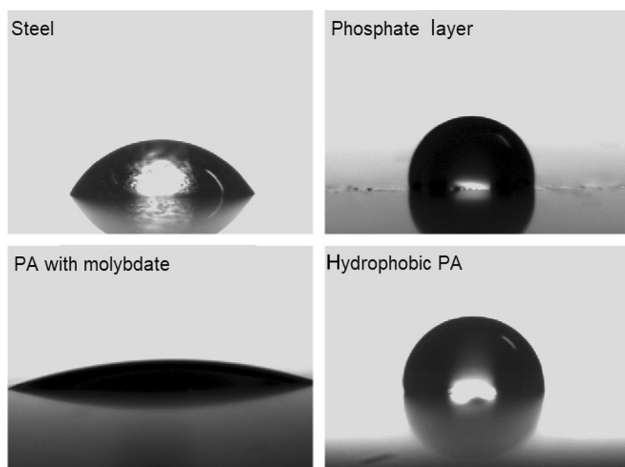
Fig. 16: Pictures of the contact angle measurements with water on the conversion layers on steel

long hydrocarbon chains arrange themselves in a direction away from the steel surface.

Surface energy

The polar σ_S^D and the dispersed σ_S^P part of the surface energy σ_s were calculated using the extended Fowkes model.[32] This method requires at least two different solvents with different polar σ_l^D or nonpolar σ_l^P characteristics to calculate the surface energy of a given solid surface. It is possible to estimate the surface energy of an unknown sample with Eqs. 1–3[32]:

$$\sigma_s = \sigma_S^D + \sigma_S^P \tag{1}$$

$$\sigma_S^D = \frac{\sigma_l(1 + \cos\theta)^2}{4} \tag{2}$$

$$\sqrt{\sigma_l^D \cdot \sigma_S^D} + \sqrt{\sigma_l^P \cdot \sigma_S^P} = \frac{\sigma_l(1 + \mathrm{Cos}\theta)}{2} \tag{3}$$

The surface energy of solid materials is dependent on the chemical composition of the surface. The results show that all samples exhibit a lower surface energy than pure PA (see Table 6). Sample 1 and sample 1 + iron oxide show the lowest surface energies. This proves that the incorporation of long C chains can lower the surface energy and the addition of iron oxide in the bath reduces the surface energy, too (sample 1 + iron oxide). The NC compounds cause by the ionic character increases the surface energy; therefore, the pure and the mixtures with NC compounds should gain only a low corrosion protective performance.

Scanning electron microscope—energy-dispersive X-ray analysis (SEM-EDX)

To prove the precipitation mechanism and especially the distribution of molybdenum-based layers and phytic acid-based layers, the elemental composition has been measured by means of SEM-EDX.

The results of the EDX measurements are illustrated in Table 7.

The elemental composition of steel shows an amount of 77% iron and furthermore, about 10% of carbon and oxygen. No significant amounts of phosphorous were observed, while on the other hand,

Table 5: Contact angle for all samples

	PA	Steel	Sample (S.) 1	S.6	S.7	S.8	S. 2/3	S. 2 + 6	S. 2 + 7	S. 2 + 8
Contact angle [°]	21.6	60.7	115	31.2	36.5	48.4	91.7	92.7	93.1	93.3

Error: +/− 8°

phytic acid shows an amount of phosphorous of about 2.2% and also a higher amount of carbon of 16.3% and a higher amount of oxygen which is about three times higher compared to the pure steel sample.

Looking at the results of the PA-alcohol samples, it can be observed that the measured amount of iron drastically decreased. Only the highest surface layer of the coated samples was measured due to the lower acceleration voltage. Furthermore, all PA-alcohol samples show phosphorous amounts of about 5% and a significantly higher carbon ratio what underlines the determined esterification of the PA.

Sample 3 showed a higher amount of iron than the PA-alcohol samples. Nevertheless, the NC products also show a decreasing amount of iron in the measured samples. Moreover, the detected amount of carbon did not change while these samples were the only ones where a nitrogen amount 2.9% could be detected.

The mixture of sample 8 and sample 2 shows a good combination of the properties of the samples on their own. A lower amount of iron was in combination with higher ratios of carbon and nitrogen. The total amount of phosphorous was around 5% while the nitrogen amount was about 2.5%.

Table 8 shows the relative ratio between PA and molybdate in the estimated conversion layers after the precipitation on the steel surface. The ratios were calculated following the assumption that each PA molecule carries six phosphorous atoms and molybdate layer unit incorporates four molybdate atoms (see Fig. 14). According to the results in Table 8, the evaluated layers mainly consist of the precipitated PA derivates. The corrosion protective behavior of molybdate layers has already been described in the literature, but the results in Table 8 lead to the conclusion that the performance of the conversion layer cannot only originate from the corrosion protective properties of molybdate but are mainly related to the properties of the used PA derivates due to the low amount of molybdate incorporated into the measured surface area.

Infrared spectroscopy

If the hypothesis of the precipitation mechanism is correct ("Synthesis products conversion coatings" section), some changes in the chemical composition in the conversion layer must be detected by means of infrared spectroscopy.

The FTIR microscope displayed the conversion layers on the surfaces with subtraction spectra. A molecular probe was selected, to prove that there are new ester groups on the surfaces, after the deposition of the layers. Figure 17 shows the infrared spectra of sample 1 and sample 2. In the range of 3000–3200 cm^{-1}, it is visible that the OH bound decreases.

Table 6: Surface energy

Sample	Contact angle (water) [°]	Contact angle (diiodomethane) [°]	Surface energy [N* cm^{-1}]
Sample 1	109.03	77.03	14.43
Sample 2	92.4	68.4	20.18
Sample 3	102.33	46.63	20.08
Sample 1 + iron oxide	112.7	76.87	13.90
Sample 8	83.73	76.87	24.01
Sample 2 + sample 8	98.13	60	19.01
PA	44.3	45	53.76
Zinc phosphated steel	102.2	49.5	19.5

Table 7: Element composition of the conversion layers on a steel surface.

Element [norm. At%]	Steel Surface	Phytic acid	Sample 1	Sample 2	Sample 3	Sample 8	Sample 1 + iron oxide	Sample 2 + Sample 8
Fe	77.7	49.3	12.5	8.4	5.17	50.4	15.4	2.2
C	11.1	16.3	52.6	56.3	47.5	13.1	43.7	55.0
O	10.5	31.1	27.6	27.8	36.9	29.2	32.2	31.6
P	0	2.2	4.5	4.7	5.4	2.3	5.9	4.7
N	0	0	0	0	0	2.8	0	2.5
Mo	0	0.6	0.5	0.4	2.2	1.5	0.9	0.7

Table 8: Samples and the respective PA to molybdate ratio in the conversion layer

Sample	PA	1	2	3	8	1 iron	2 + 8
PA/molybdate ratio	71/29	86/14	89/11	62/38	51/49	81/19	82/18
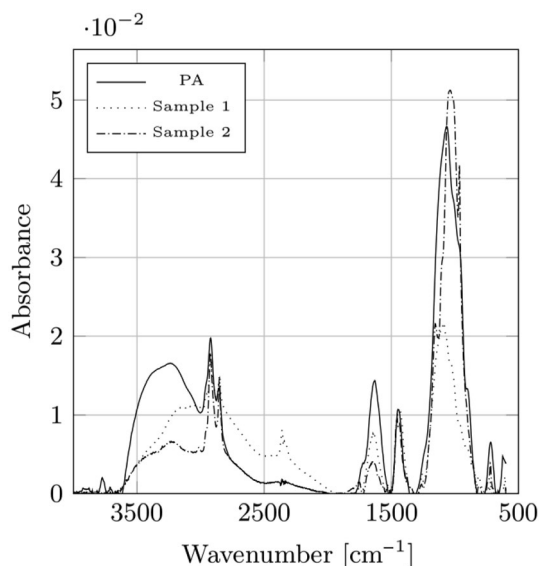
Fig. 17: Infrared spectra of the sample 1 and sample 2 conversions
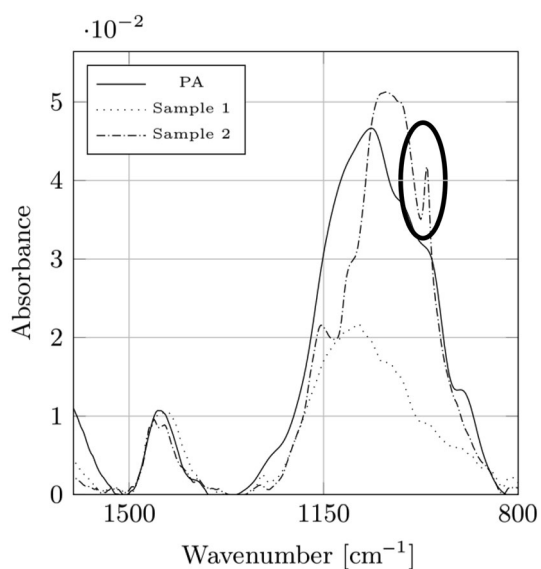

Fig. 19: IR spectra of the conversion layer with different iron concentrations from sample 1

Fig. 18: Magnified infrared spectra of the sample 1 and sample 2 conversions
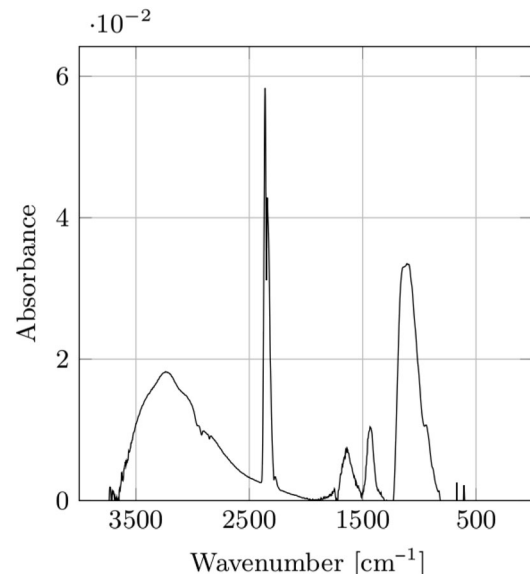
Fig. 20: IR spectrum of sample 6 on steel

This also proves that the deposition was successful because the OH groups are now bonded ionically to the iron ions. Moreover, the P–O stretch and P–O–C stretch shifted to lower wavenumbers compared to the pure PA layer.[8,33]

These spectra were magnified in Fig. 18. The results prove that the measured layers on the surface involve double bonds, which leads to the conclusion that the undecen-1-ol was successfully incorporated into the product molecules The characteristic peak of the C–H "out-of-plane" deformation vibration for C=C double bonds is visible at 970–960 cm^{-1}.[7] This peak only

shows up for sample 2 which includes the double bond probe. The same peak can be found for the liquid products spectra (see "Appendix IR-Measurements"). It should be mentioned that the surfaces were cleaned with solvents to prove that no unbounded alcohol was measured. Therefore, the proof of the covalent hydrophobic modification and the precipitation without changes of the molecules could be done by means of infrared spectroscopy (Fig. 18).

Furthermore, the bath was modified with different concentrations of metal oxides [cerium(IV) oxide, manganese(II/III) oxide, manganese(IV) oxide, and iron oxide] to decrease the amount of free P–OH groups, increase the network density by a higher

717
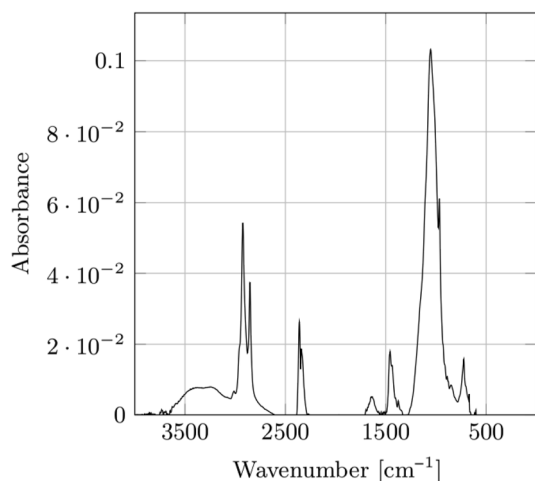
Fig. 21: IR spectrum of sample 6 + sample 2

Table 9: Cyclic voltammetry data

Sample	Slew rate dU/dt	Charge/ μC	Coverage/ %
Steel	100	372.57	0
PA	10	179.09	96
Sample 1	10	240.11	94
Sample 2	10	134.76	94
Sample 3	10	120.19	89
Sample 1 with iron oxide	10	124.33	94
Sample 6	10	245.90	84
Sample 7	10	368.84	82
Sample 8	10	286.88	78
Sample 8 + sample 2	10	201.19	94
Sample 7 + sample 2	10	100.59	96
Sample 6 + sample 2	10	93.14	96

Error$_{Coverage}$ ± 7%

Table 10: Bandgap of the samples according to the Tauc plot

Sample	Bandgap [eV]
Sample 2	3.2
Sample 6	1.8
Sample 7	2.1
Sample 8	2.3
Sample 2 + sample 6	3.6
Sample 2 + sample 7	3.3
Sample 2 + sample 8	3.2

amount of crosslinking and an increase of the hydrophobicity. The following IR spectra (Fig. 19) show the peak changes for different amounts of iron oxide in a 100 mL dip bath (see "Appendix Other spectra" spectra, Fig. 69). The respective PA derivate in these dip baths was sample 1.

The OH peak (3200 cm^{-1}) was the lowest for a total amount of 0.05 g of iron oxide in the bath solution. After this point, the OH peak started to increase for an increasing amount of iron oxide. Different concentrations were tested for all metal oxides (see Fig. 19 and "IR measurements" Figs. 40, 41, 42, and 43). All oxides showed the highest reduction of the OH peak at 0.05 g. For this reason, this quantity was used for the next steps. Iron oxide, a harmless material, showed good results in the SST (see below) and has ideal solubility properties compared to the other metal oxides, which also performed well in the SST but showed poor solubility.

Figure 20 and "IR measurements" (Figs. 38 and 39) show the NC products on the steel surface. The spectra are an indicator that the PA-NC products were successfully precipitated on the steel surfaces. The IR spectra of the NC products show the characteristic P–OH peak of PA at 950 cm^{-1} and the NH$_2$ peak of the nitro compounds at 1500 cm^{-1}. Figure 20 shows the surface spectra of sample 6. It can be observed that the conversion coated steel surface shows the same characteristic peaks as the pure product. This proves that both products were precipitated. The spectra of samples 7 and 8 and their mixtures are illustrated in the appendix ("IR measurements" Figs. 34, 35, 36, 37, 38 and 39).

In the next step, mixtures of the alcohol products and NC products were validated. The NC products carry many reactive groups which could cause a better surface adhesion, and the alcohol products show high contact angles which could also have a positive effect on the adhesion. Different quantity compositions were tested, but this had no influence on the coating itself. For the following tests, we used a proportion of 50/50 (alcohol product/NC product).

Figure 21 shows the IR spectra for the mixture of product samples 2 and 6. This example was chosen because of the incorporation of double bonds in sample 2. This allows observation to determine if the products are still successfully precipitated on the steel substrates.

It is apparent that the double bond peak from sample 2 and the NC peak at 1500 cm^{-1} can be observed for the mixture. This was repeatable for all mixtures.

Cyclic voltammetry

The total electrochemical surface coverage of the phytic acid layers was investigated using cyclic voltam-
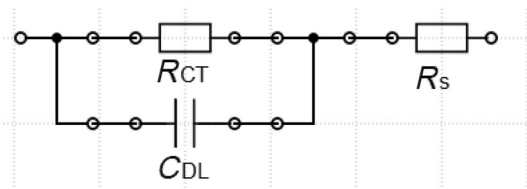
Fig. 22: Randles plot
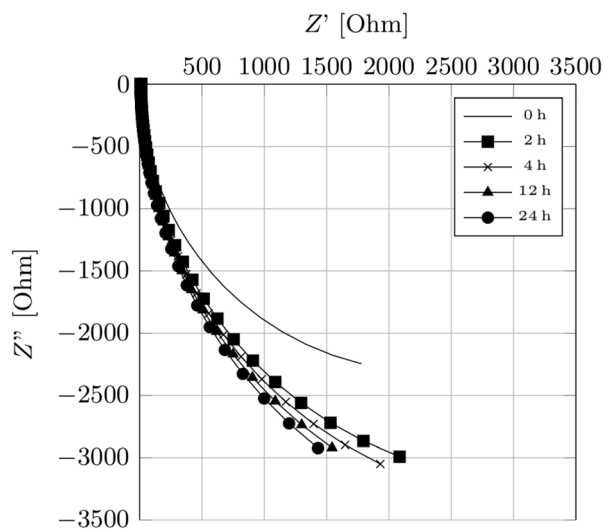
Fig. 23: Nyquist plot of sample 2 at different times
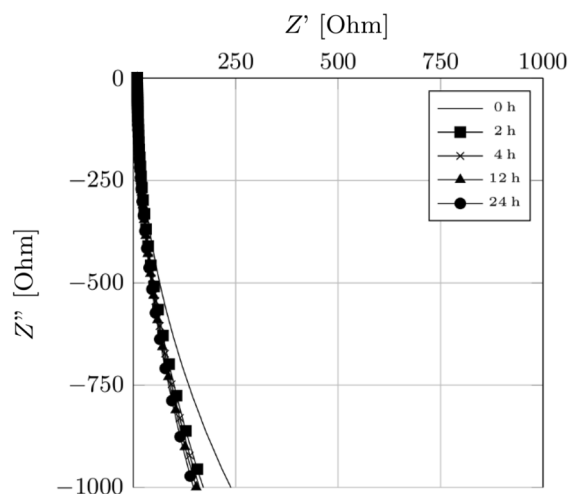
Fig. 24: Zoomed-in Nyquist plot of sample 2 at different times.

Fig. 25: Capacity from the simulation with the Randles equivalent circuit versus time
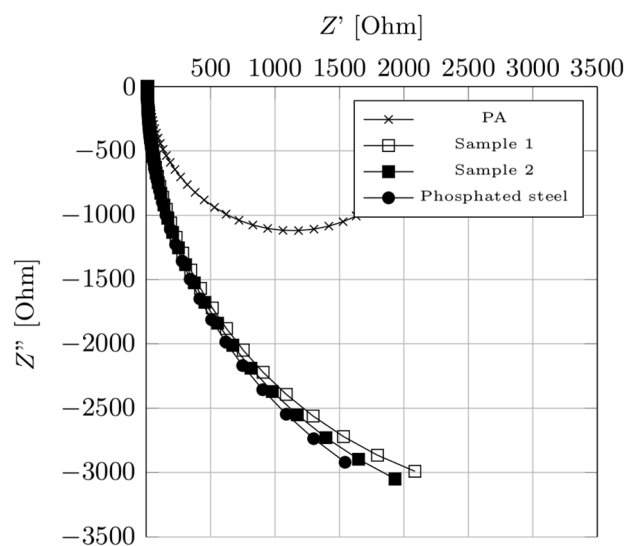
Fig. 26: Nyquist plot at *t* = 0 of the measurements.

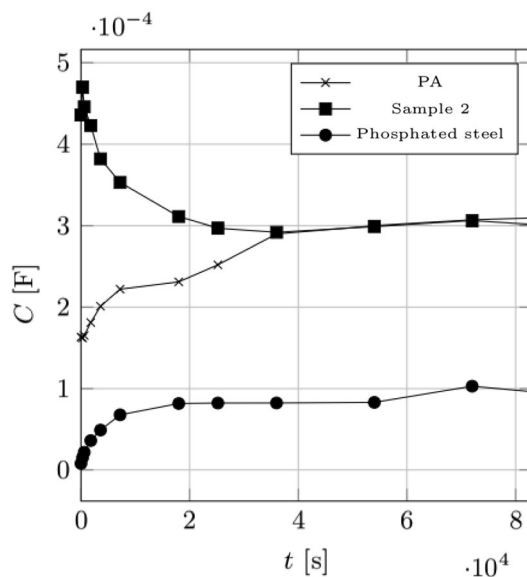metry as described in literature.[34,35] Based on the hypothesis of the precipitation based on an autophoretic process, a surface coverage of 100% is impossible in principle because a free surface is necessary for anode and cathode reaction to gain the pH increase near the surface. Nevertheless, a value near 100% has to be achieved for a high-level corrosion protection property.

The total surface coverage was measured with noncoated steel as a reference sample. The Randles Sevcik equation (Eq. 4) was used to convert the current density for steel to a unified scan rate. With the

Table 11: Simulated EIS data

Sample	Start			After 24 h		
	R_s [Ohm]	R_{CT} [Ohm]	C_{DL} [μF]	R_s [Ohm]	R_{CT} [Ohm]	C_{DL} [μF]
PA	18.5	2.20 K	163	15.2	7.80 K	319
Sample 1	11.6	14.8 K	123	12.6	13.6 K	135
Sample 2	12.0	2.77 K	436	11.3	10.2 K	301
Phosphated Steel	19.9	2.95 K	7.83	13.4	17.7 K	94.3
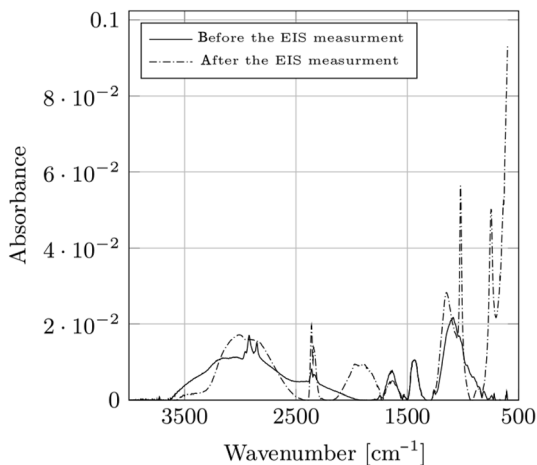
Fig. 27: Corrosion products after 24 h of EIS for sample 1
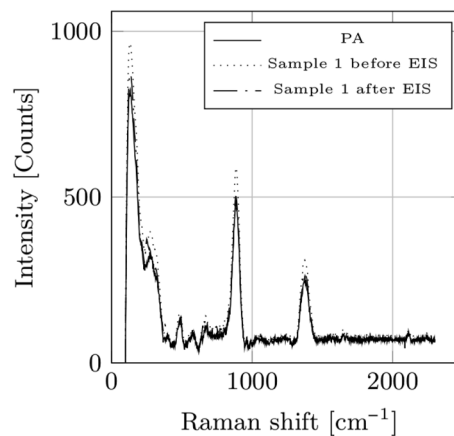
Fig. 28: Raman spectra of PA and sample 1

calculated current density of steel, it was possible to estimate the total surface coverage using (Eq. 5).

Randles Sevcik[34]:

$$i_{\mathrm{Peak}} = \pi^{\frac{1}{2}} n F \left(-\frac{\alpha n F}{RT} \upsilon \right)^{\frac{1}{2}} \left(\frac{\alpha n F}{RT} \upsilon t \right) 0.282 D_{\mathrm{Red}}^{\frac{1}{2}} c_{\mathrm{Red}}^{0}$$
$$= 3.01 \cdot 10^5 n^{\frac{3}{2}} D_{\mathrm{Red}}^{\frac{1}{2}} c_{\mathrm{Red}}^{0} \upsilon^{\frac{1}{2}} \alpha^{\frac{1}{2}} \tag{4}$$

i_{Peak}, maximum current [A/cm^2]; n, number of exchanged electrons; D_{Red}, diffusion constant [cm^2/s]; c_{Red}^{0}, concentration of S_{Red} at $t = 0$ and $c_{Ox} = 0$ at $t = 0$; υ, scan rate [V/s]; α, transition factor.

$$\Theta = 1 - \frac{Q_{\mathrm{coated}}/A_{\mathrm{coated}}}{Q_{\mathrm{Steel}}/A_{\mathrm{Steel}}} \tag{5}$$

[Θ]: degree of coverage, [Q]: charge and [A]: area

The coverage of sample 1 is the lowest (see table 9). Pure phytic acid had a surface coverage of around 96%, while samples 1–3 and samples 1 + iron oxide and the mixtures with sample 2 showed the same coverage between 94 and 96% of the total surface. The results of the samples 1 and 1 + iron oxide show that the addition of iron oxide led to no difference for the total surface coverage.

The products made with NC (sample 6–sample 8) exhibited a relatively low surface coverage, where

sample 8 shows by far the worst results with 78%. These results correlate with the results of the salt spray test, i.e., a high surface coverage gains a high corrosion protective property.

Bandgap by Tauc plot

A conversion layer has to fulfill two demands. First, the layer must increase the adhesion of the organic coating layer and second it should inhibit the galvanic coupling between anode and cathode on the substrate to decrease the corrosion rate at the surface.[34]

Only an insulating layer can inhibit the galvanic coupling, and therefore, the investigation of the bandgap of the conversion layers has to be performed.

The extension of the linear slope in the Tauc plot of the UV–VIS spectrum of sample 2 leads to a bandgap of approximately 3.2 eV (see Table 10 and "Appendix Bandgap").[34,36] The spectra were plotted according to the Kubelka–Munk equation. The same procedure was repeated for the other samples.

Materials with bandgaps between 0.1 and 1.5 eV are semiconductors. For the best corrosion protection, nonconducting materials with a bandgap bigger than 3 eV are needed. All samples with alcohol as well as the mixtures behaved as nonconductors while pure NC compound layers were semiconductors. These results correlate with the SST results.
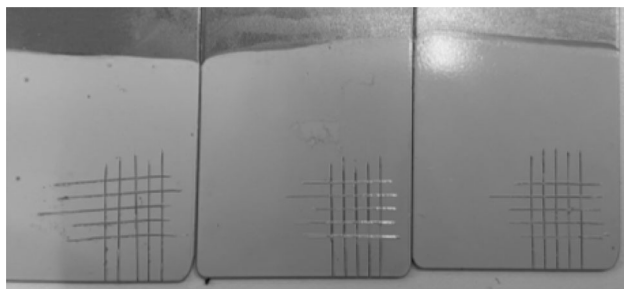
Fig. 29: Dry crosscut test from the treated sample 2 with E-coat
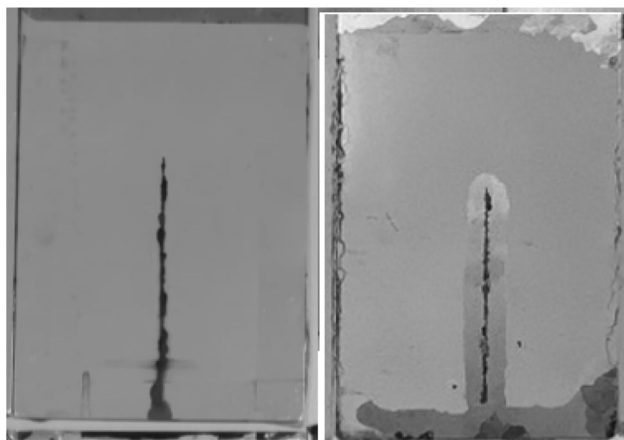
Fig. 30: Sample 1 after 500 h and 650 h SST

Electrochemical impedance spectroscopy

As shown in the "Contact angle" section, the surface of the modified phytic acid layers is hydrophobic, in "Bandgap by Tauc plot" section, a high surface coverage could be detected, and in "Electrochemical impedance spectroscopy" section, it is shown that the conversion layers are insulating. Therefore, the conversion layers should be gaining a high electrochemical barrier against corrosion proved by means of electrochemical impedance spectroscopy as follows.

ELECTROCHEMICAL MEASUREMENTS: Electrochemical impedance spectroscopy (EIS) was used to determine the barrier properties of PA and its modifications. All measurements were carried out at least three times to validate the measured data. The treatment of the surface in NaCl solution at atmosphere should show corrosion processes or changes of the conversion layers.[37]

The EIS measurements were fitted with the Randles plot (see Fig. 22). The Randles equivalent circuit[38] is the simplest possible model to describe coated metal surfaces. The fitting error of the Randles fit was 3.6% $\pm$ 0.5% for all models. The circuit plot consists of a series connection from a charge resistance impedance (R_{CT}) and the Warburg impedance (Z_D). On the

Fig. 31: Sample 1 with different oxides after 500 h SST in the following order from the top left to the bottom right [phosphated steel, Sample 1, Ce(IV), Mn(II/III), iron oxide]

opposite side of the circuit is the double-layer capacity (C_{DL}). These are all connected in series with the electrolyte resistance (R_S)[38,39] (Fig. 23).

Figure 23 shows the Nyquist plots (corresponding Bode plots in the appendix Figs. 54, 55, 56, 57, 58, 59, 60, and 61) of sample 2 at different times. The results show a changing semicircle without clear corrosion processes such as a Warburg impedance. These results are a significant improvement compared to the stabilities recorded for pure PA layers (see example in the literature[2]). Figure 24 shows close ups of Fig. 23. The plots show that no development of a second semicircle occurred, even though it was expected that a second semicircle would occur due to corrosion processes on surface areas which are not covered with the conversion coatings.[39,40] All plots show semicircles.

Moreover, the capacity based on the model with the equivalent circuit (Fig. 25) was plotted against the time and the results were compared with the ones of the phosphated steel. A sharp decreasing of the capacity at the beginning of the measurements of the PA derivate, which originates from the usage of the Randles plot, shows that at the start corrosion occurs on these samples. This corrosion process happens at noncovered surface and ends when the corrosion products put the surface into a passive state (see Fig. 32). This behavior shows that the conversion layer itself is stable (within these 24 h) and it also underlines the Raman results (see below).

Figure 26 (corresponding Bode plots in the appendix Figs. 54, 55, 56, 57, 58, 59, 60, and 61) shows the semicircles of all samples at $t = 0$. The direct comparison demonstrates that the layers of the PA-products have a clearly higher barrier resistance than the PA or the zinc phosphated steel. The value of Z'' increases from low to high in the order: PA, zinc phosphate, sample 2 to sample 1.

The results in Table 11 underline these observations. At the start of the measurements, the phosphated steel sample shows the lowest capacity of all samples which means that the barrier resistance of the phosphated steel samples was the highest at $t = 0$ while sample 1 had the second highest value. After 24 h of measurement, phosphated steel still has the highest barrier resistance but the measured value is about 12 times lower as at the beginning while sample 1 is still at nearly the same value as in the beginning and the results are comparable to the values measured for the phosphate layer. These results are noticeable because they underline that the long-term barrier resistance of the sample−1-PA derivate is comparable to the resistance of phosphated steel while the degree of reduction was lower during our experiments. The PA reference and sample 2 did not show such a high barrier resistance as phosphated steel or sample 1. Both had significantly lower contact angles at the start and at the end, but it is noticeable that the barrier resistance of sample 2 increased due to ongoing passivation of the surface in the first 24 h while the PA layer lowered the resistance even further because the layer behaved too hydrophilic.

The overall results show that the phytic acid derivates are very stable within the first 24 h in NaCl solution. This can also be observed in the results of the SST, where the decreasing wet surface adhesion is a bigger problem than the occurring delamination. The results of the NC products and mixtures show the same results (see Appendix spectra "EIS spectra").

Furthermore, the corrosion products formed on the uncovered surface areas were measured after the treatment with 3% NaCl for 24 h. The associated IR spectra are shown in Fig. 28. The data show a γ-FeOOH peak at 1018 cm^{-1} from the OH– stretch.[34] At 740 cm^{-1}, a Fe(OH)$_2$ peak developed.[34] From 2500 to 3200 cm^{-1}, a strong band resulting from the availability of the involved water occurred, which can exactly be described through the O-H in H-bridge to P–OH groups.[34] At 1000 cm^{-1}, the PA peak was detected in both cases, before and after the EIS measurements, which shows that the conversion layers did not vanish during the measurements (see Fig. 27) and the uncovered surface areas are covered rapidly with corrosion products which finally gain a stable conversion layer against corrosive treatment.

Moreover, the Raman spectra show the deposited conversion layers and their boundary layers on the surfaces (see Fig. 28), too.

The peak at 860 cm^{-1} represents the RO–P=O bound and the peak at 1350 cm^{-1} represents the aromatic ester bonds, which can be found in both, the nonmodified PA and the modified PA.[8,33] The Raman spectrum after the EIS measurement of sample 1 shows the same peaks as before, which proved that the conversion layer was stable after the treatment with the NaCl solution. It can also be observed that the peaks decrease after the EIS measurement. This leads to the conclusion that the conversion layer had noncoated areas which corrode, but not enough that the corrosion products are visible in the Raman spectra (see Fig. 28).

Salt spray and crosscut test

Standard neutral SST was used to determine the corrosion protective properties of the hydrophobic PA conversion layers in combination with an organic coating. The samples are coated with a so-called cathodic dip coating (E-coat), which is the most used standard coating for corrosion protection. The test duration was 500 h or 650 h. The degree of delamination was observed according to DIN EN ISO 4628-8.

The crosscut test (DIN EN ISO 16286-2) was the first test to evaluate the surface adhesion of the E-coat on the conversion layers in dry state. All layers showed a crosscut classification between the classes 0 and 1, which is on one level with the zinc phosphated reference steel plate that displays the current industrial standard. All samples are tested with a pull-off test, too, but even the bare steel sample shows a higher adhesion to the E-coat than the adhesive used to fix the stamp. Therefore, the adhesion is based on the organic coating and could hardly be influenced by the conversion layers in the case of E-coats.

In the SST, all samples showed a good performance and no significant delamination after 500 h although delamination started after 650 h. Pictures of the treated samples after the crosscut test are shown in Fig. 29.

The salt spray test of the new hydrophobic layers after 500 h showed a good performance and underlined the good results. After 650 h of salt spray test, the PA layers showed corrosion in the areas around the defect (see Fig. 30). For more colored pictures, see appendix spectra "Salt spray test."

After addition of the oxides to the bath, a salt spray test was performed. After 500 h of testing, none of the samples showed visible delamination. The corrosion protective behavior of the samples with metal oxides outperformed even phosphated steel (top, left) or sample 1 (top, right) without the additionally added oxides. Sample 1 showed a corrosion of 0.8 mm, phosphated steel of 0.5 mm at the scratch according to DIN EN ISO 4628-8 and for the samples with additional oxides 0.05 mm [bottom, left to right; cerium (IV), manganese (II/III), iron (III)]. These results prove that the addition of metal oxides can lead to a significant enhancement of the corrosion protective properties. A higher amount of iron in the layer

Table 12: Delamination and corrosion after SST

Ø	Sample 6	Sample 7	Sample 8	Steel	Phosphated steel	Sample 2
Delamination [mm]	5.3	6.0	19.8	8.9	0	12.2
Corrosion [mm]	0.3	0.3	0.5	0.8	0.2	0.5

Ø	S. (Sample) 2 + S.6	S.2 + S.7	S.2 + S.8	S.1 + S.6	S.1 + S.7	S.1 + S.8	S.3 + S.6	S.3 + S.7	S.3 + S.8
Delamination [mm]	2.2	2.1	1.7	5.3	8.6	5.1	3.0	6.6	1.9
Corrosion [mm]	0.3	0.3	0.2	0.3	0.3	0.3	0.3	0.2	0.1
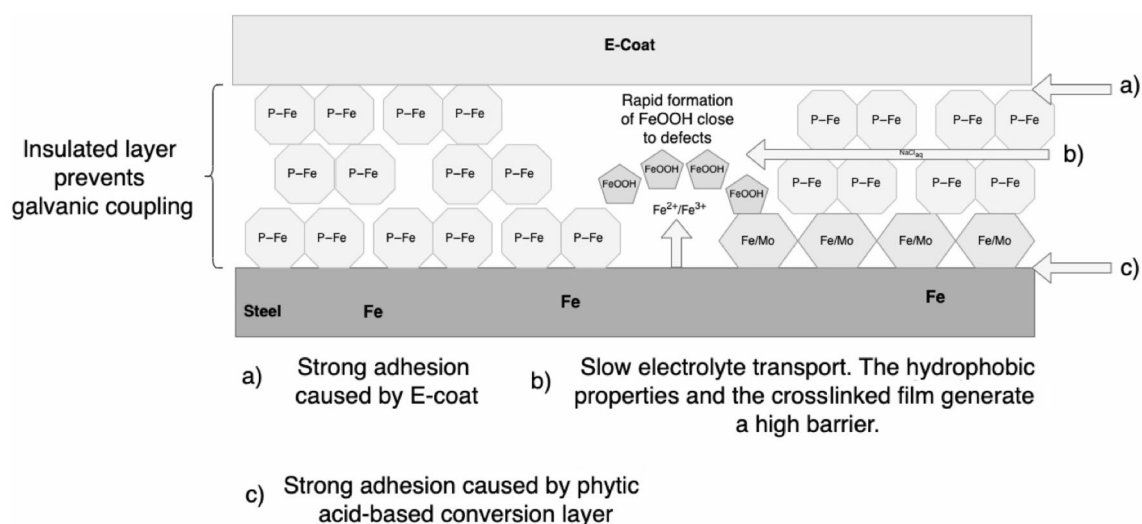
Fig. 32: Corrosion protection mechanism of the E-coated conversion layer

causes a higher crosslinking and high hydrophobicity which decreases the electrolyte transport through the coating. However, all metal oxides show the same outstanding results but iron oxide as a cheap and nontoxic compound should be the metal oxide for further investigations (see Fig. 31).

Table 12 illustrates an overview for the delamination and corrosion protective properties for the PA-NC samples and mixtures. The corrosion is regarded as the broadness of the occurring rust and the delamination as the peeling off of the coating underneath the cut. After 650 h of SST, all spectra are in appendix spectra "Salt Spray Test."

The results of the salt spray test already showed a low corrosion rate. In samples 6–8, only the NC products as well as the alcohol-only products already granted good corrosion protection, but delamination occurred for all samples. The bad results for the NC products show a correlation with the results of the surface coverage (see Table 9) and the bandgap results

(see Table 10). The best results were achieved with the product mixtures. Especially sample 8 showed a good corrosion protection, while the delamination was significantly reduced.

The corrosion protective mechanism is summarized in Fig. 32. The excellent corrosion protective performance of the hydrophobic modified phytic acid-based conversion layer in combination with E-coats is based on several effects proved with technical, spectroscopic, and electrochemical methods. The strong adhesion to the substrate has been proved with crosscut test and pull-off test, whereas the adhesion to the E-coat is caused by the E-coat itself (see above). The high bandgap of the layer measured with UV–VIS spectra illustrated the insulated properties of the layer which reduces the galvanic coupling. The hydrophobic properties based on the chemical modification of phytic acid and proved with contact angle measurements reduce the transport of electrolyte into the interface to initiate corrosion processes. The crosslinking of the film caused

by the high functionality of phytic acid improves the barrier against the electrolyte as shown with EIS. And finally, the slow uncovered surface of around 5% proved with CV enables an initiation of corrosion but the defects are rapid closed by corrosion products measured with EIS. The formation of FeOOH detected with IR and Raman spectroscopy gains a dense layer without an interface between the FeOOH layer and the conversion layer, which may be caused by reaction of free P–OH groups of the layer with the corrosion products.

Conclusions

The current industrial need for green alternatives to conventional harmful technologies is as big as ever before. Even though there is much research in this field, no comparable and green alternative for conventional conversion technologies has been discovered until today.

Previous studies suggested PA as a potential raw material for new conversion layers, but all authors concluded that the hydrophilic nature decreases the compatibility with organic coatings and the anticorrosion properties,[2] although PA itself showed good compatibility with different metal surfaces[41,1] and was able to enhance corrosion resistance on the respective surfaces compared to blank substrates but was not able to completely suppress corrosion which made further corrosion protection necessary.[10] Our recent results showed that a suitable modification of PA can overcome these downsides. PA-alcohol and amine products in our study showed increased contact angles, enhanced corrosion protective properties, and excellent coating ability with organic coatings. The results show that hydrophobic PA-based conversion layers could be a green alternative to conventional phosphate corrosion protection pretreatments for steel without the use of zirconium or titanium compounds.[42] The spectroscopic data proved that it is possible to modify PA with OH-functional reaction partners and the proposed autophoretic precipitation mechanism could be proved, too.

The hydrophobicity and therefore the coatability of the conversion layers is directly dependent on the incorporated functionality of the used alcohols/fatty alcohols. The modification of the PA led to a significant increase in the corrosion protective behavior, which could be proven through EIS and SST measurements.

The performance of the hydrophobic phytic acid conversion layers could be improved by the addition of iron oxide in the dip bath to increase the network density of the layer, decrease the amount of polar P–OH groups proved by spectroscopic and electrochemical methods, and finally lead to better results in the SST.

Finally, the results illustrated that the combination of spectroscopic, electrochemical, and technical tests allows description of the corrosion protective mechanism of conversion layers.**Funding** Open Access funding enabled and organized by Projekt DEAL.

Appendix

IR measurements

See Figs. 33, 34, 35, 36, 37, 38, 39, 40, 41, 42, and 43.
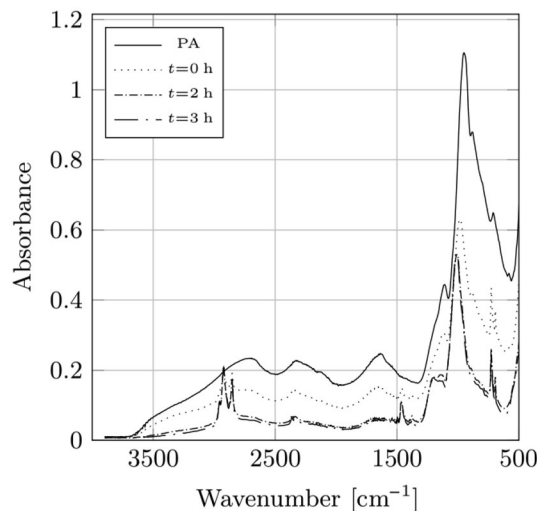
Fig. 33: ATR spectra during the synthesis of sample 1
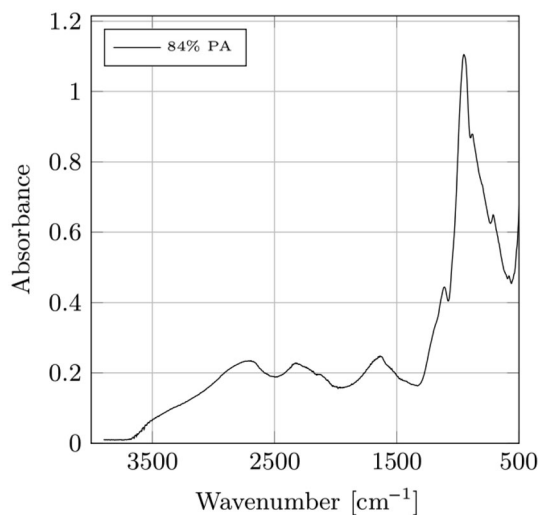
Fig. 34: IR spectrum phytic acid 84%
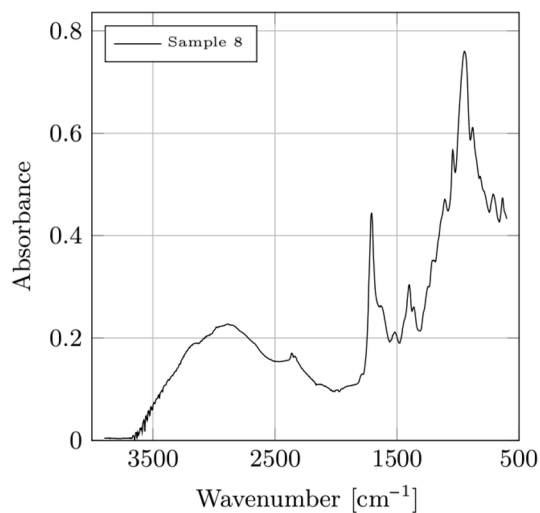
Fig. 37: IR spectrum from sample 8
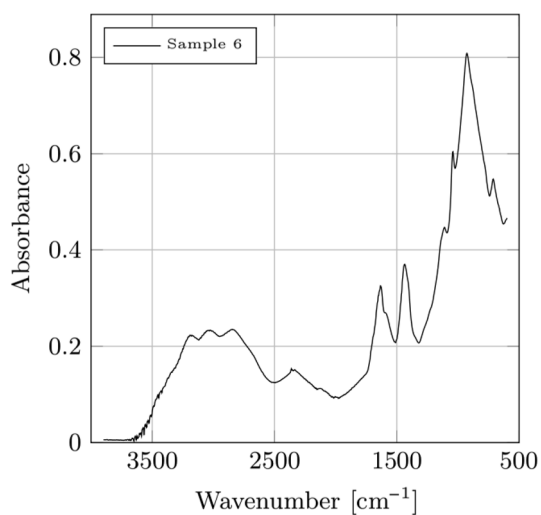
Fig. 35: IR spectrum from sample 6
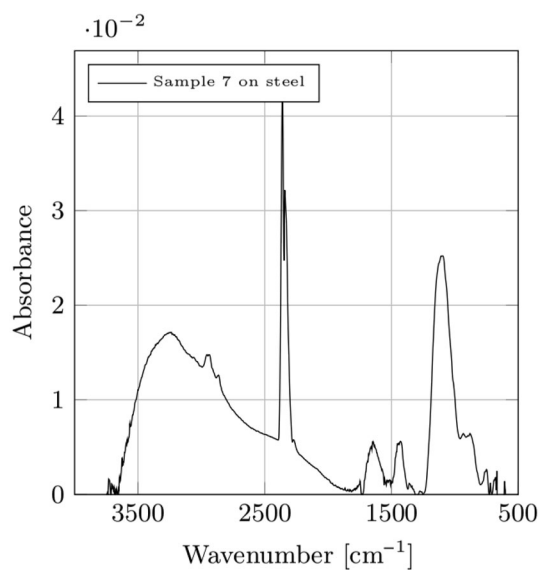
Fig. 38: IR spectrum from sample 7 on steel
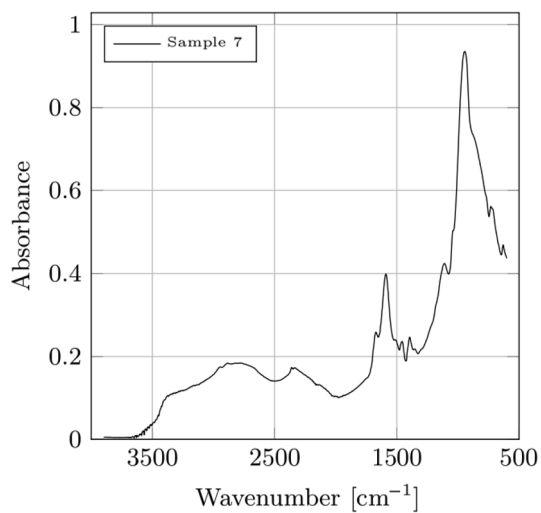
Fig. 36: IR spectrum from sample 7
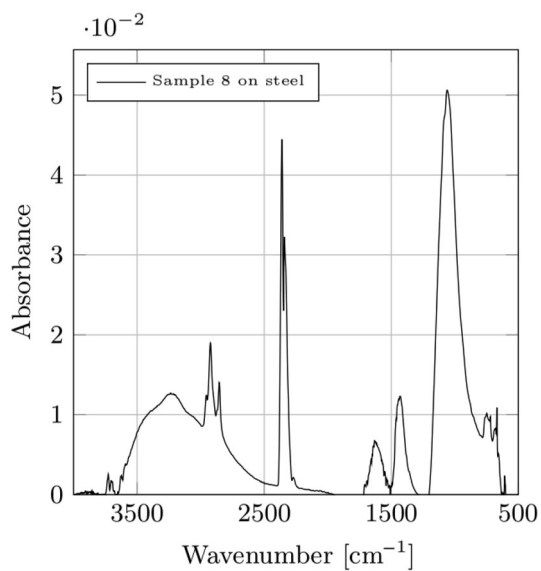
Fig. 39: IR spectrum from sample 8 on steel
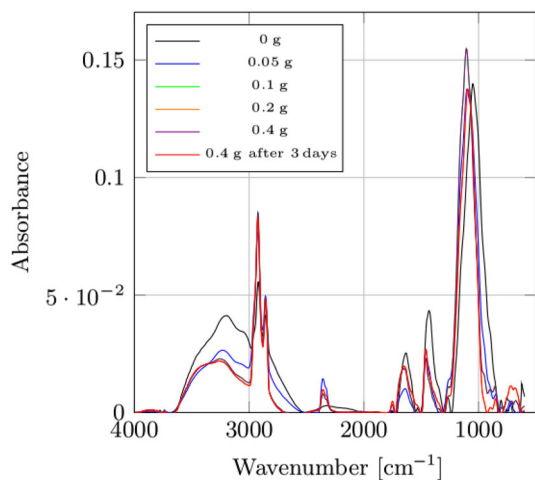
Fig. 40: IR spectra from sample 1 with Ce(IV)
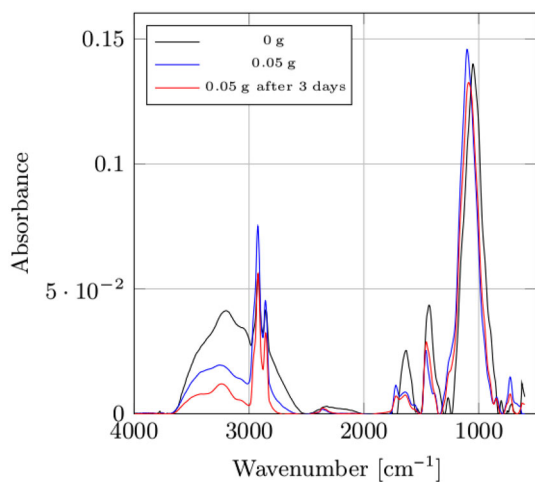
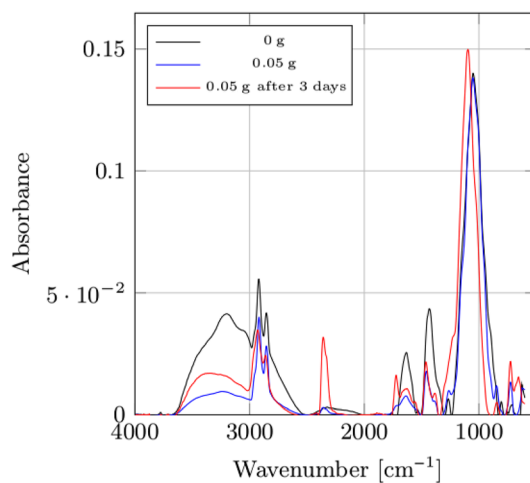**Fig. 41: IR spectra from sample 1 with manganese II/III**
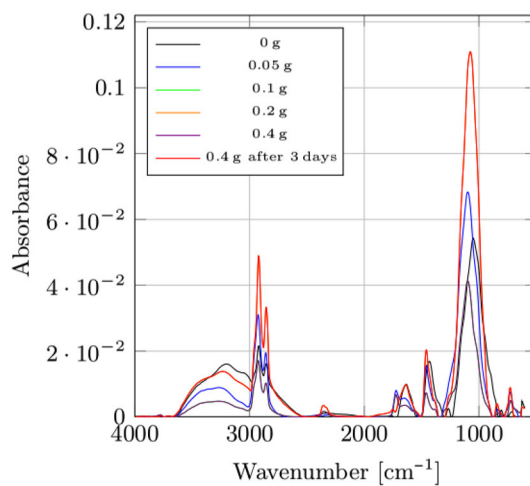

Fig. 42: IR spectra from sample 1 with manganese IV

Fig. 43: IR spectra from sample 1 with zinc oxide

NMR spectra

See Figs. 44, 45, 46, 47, 48, 49, and 50.
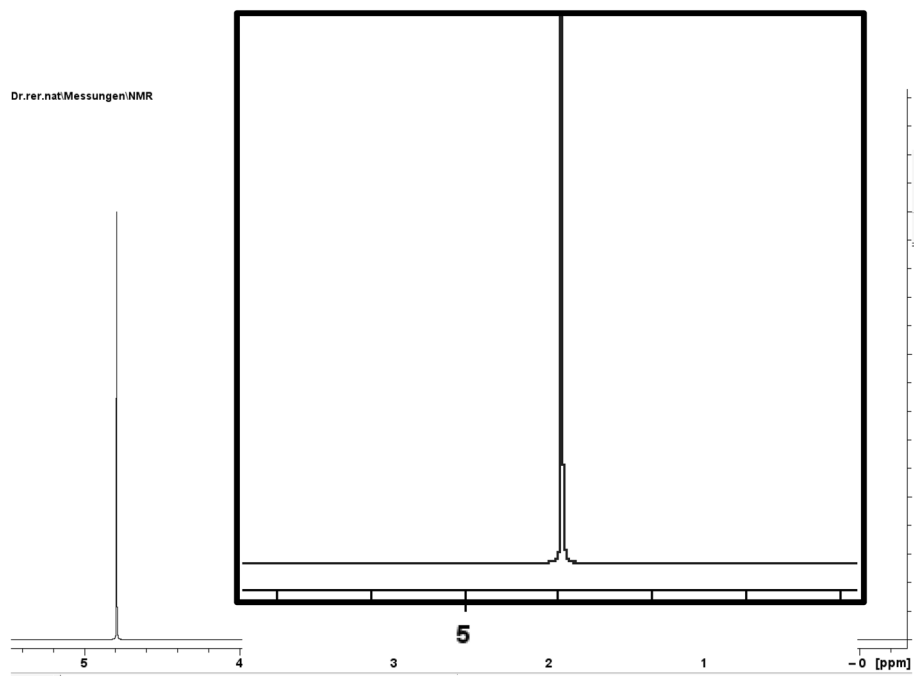
Fig. 44: ^{1}H-NMR spectrum of PA
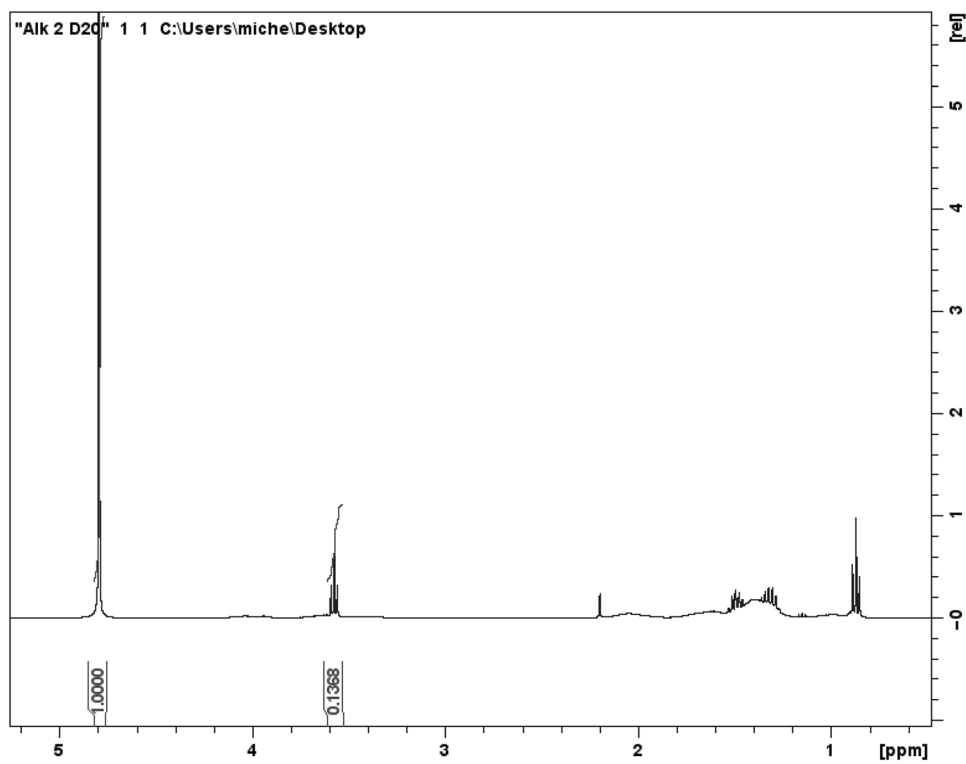
Fig. 45: ^{1}H-NMR spectrum of sample 2
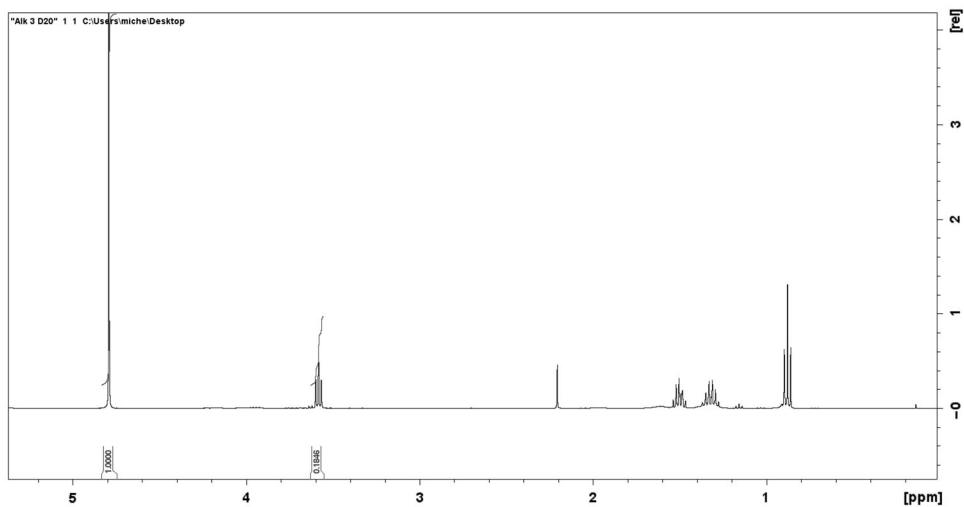
Fig. 46: ^{1}H-NMR spectrum of sample 3
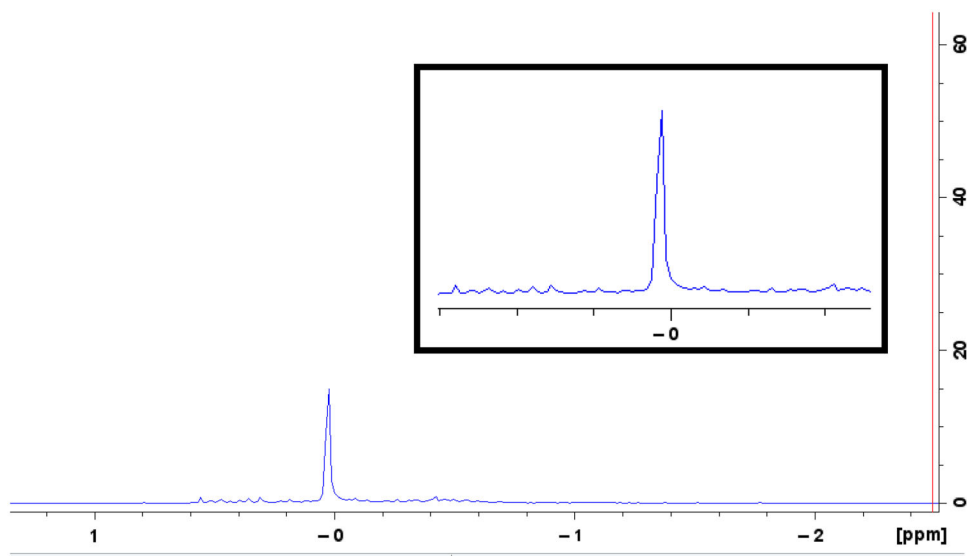
Fig. 47: ^{31}P-NMR spectrum of PA
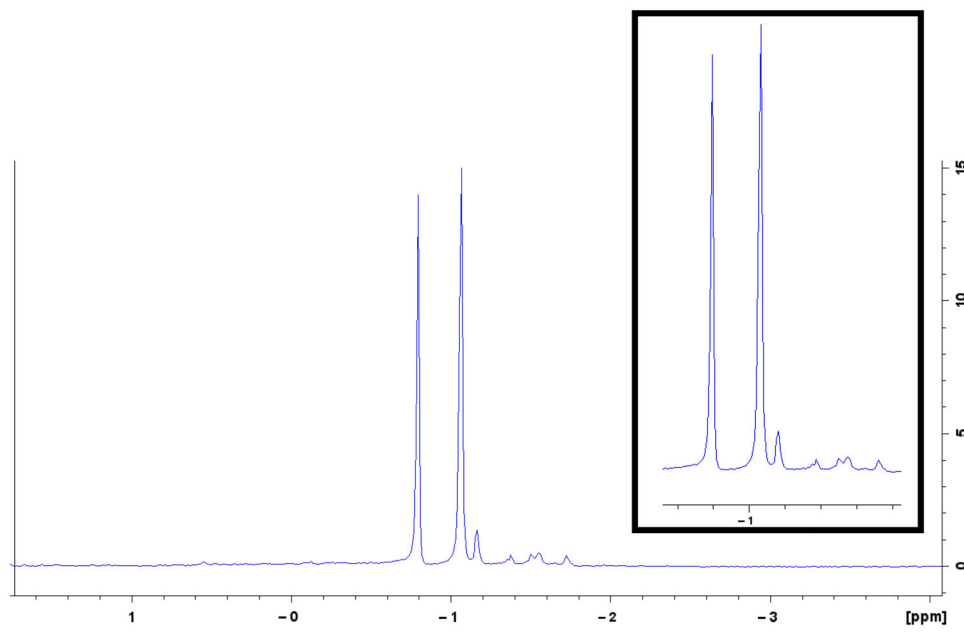
Fig. 48: ³¹P-NMR spectrum of sample 3
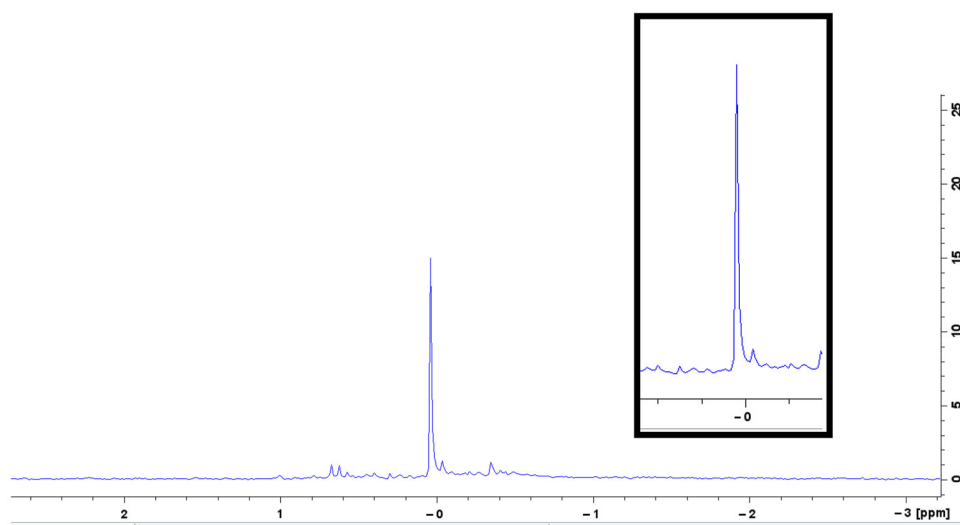
Fig. 49: ³¹P-NMR spectrum of sample 2
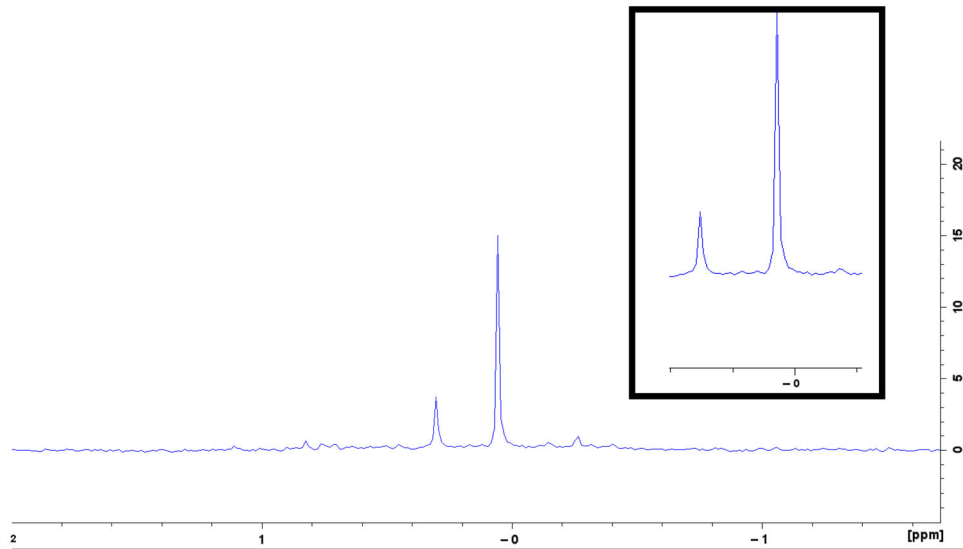
Fig. 50: ^{31}P-NMR spectrum of sample 1

EIS spectra

See Figs. 51, 52, 53, 54, 55, 56, 57, 58, 59, 60, and 61.
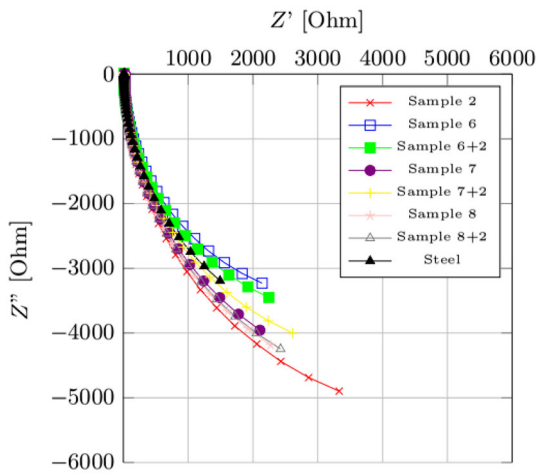
Fig. 51: Nyquist-plot spectra at 0 h
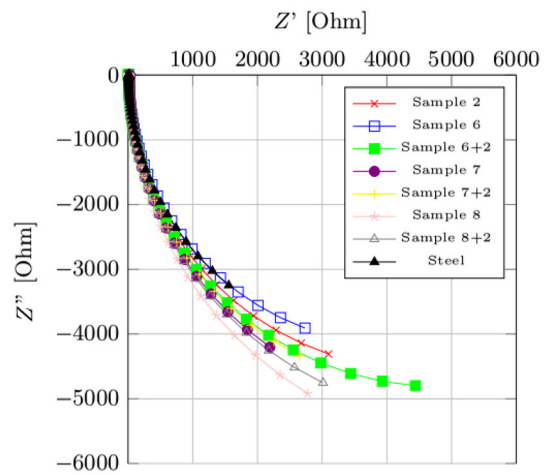
Fig. 52: Nyquist-plot spectra at 1 h
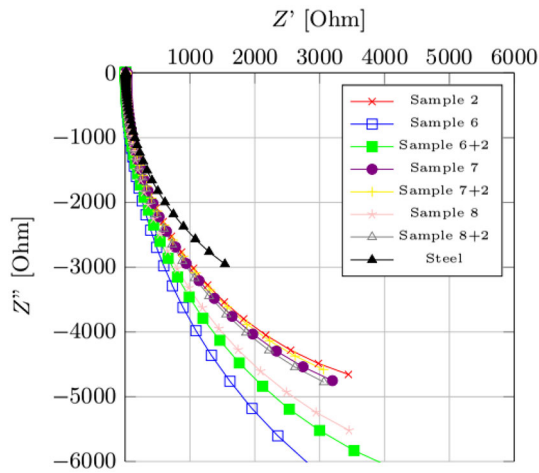
Fig. 53: Nyquist-plot spectra at 24 h
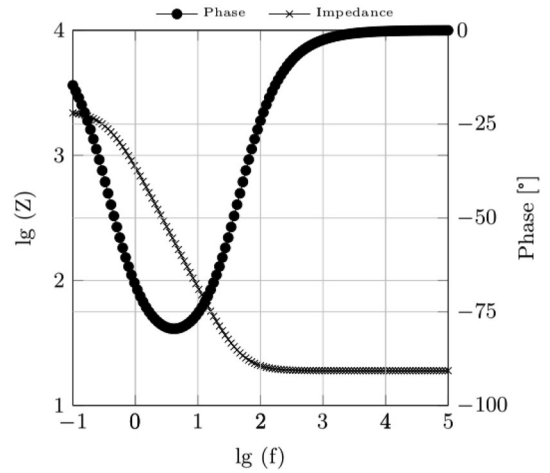
Fig. 56: Bode-plot spectra of PA, *t* = 0 h
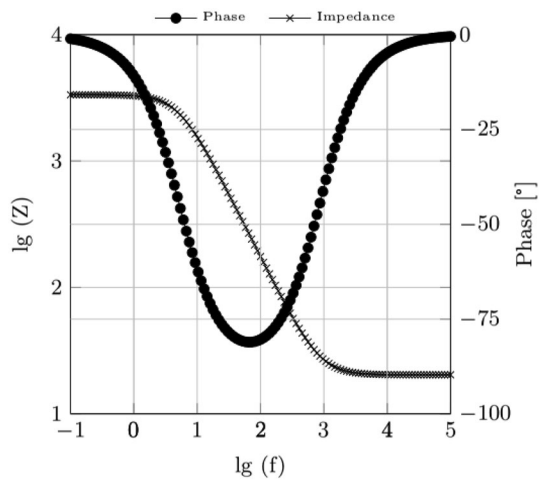
Fig. 54: Bode-plot spectra of phosphated steel, *t* = 0 h
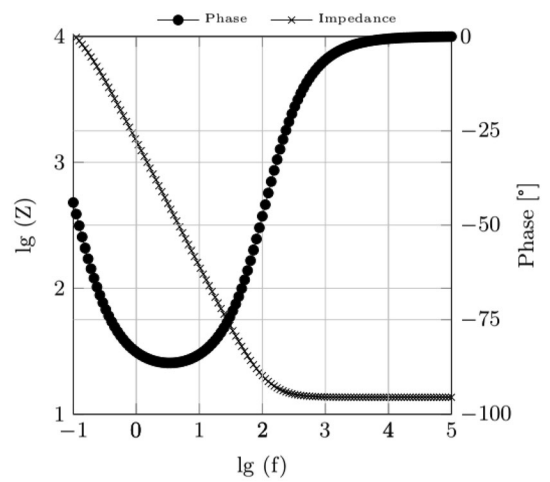
Fig. 57: Bode-plot spectra of PA, *t* = 24
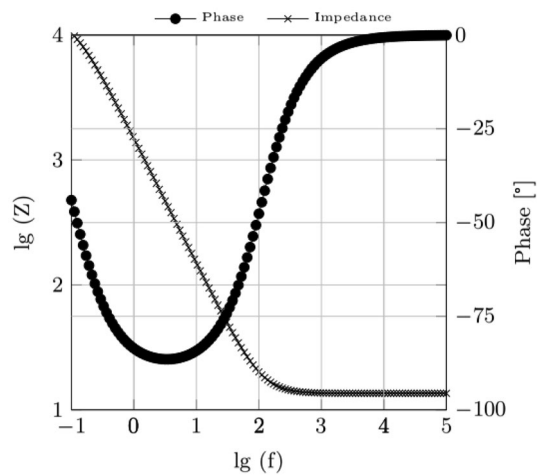
Fig. 55: Bode-plot spectra of phosphated steel, *t* = 24 h
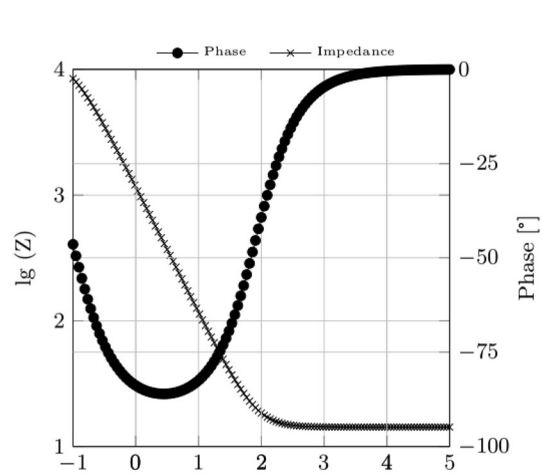
Fig. 58: Bode-plot spectra of sample 1, *t* = 0 h
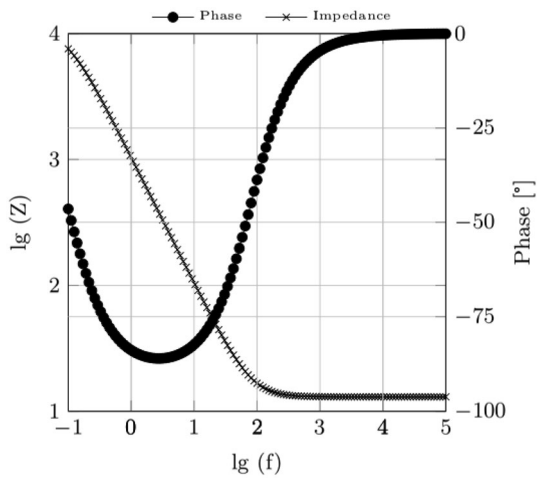
Fig. 59: Bode-plot spectra of sample 1, *t* = 24 h
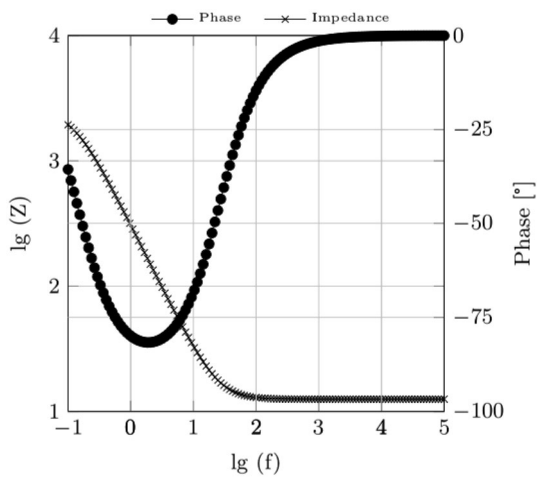
Fig. 60: Bode-plot spectra of sample 2, *t* = 0 h
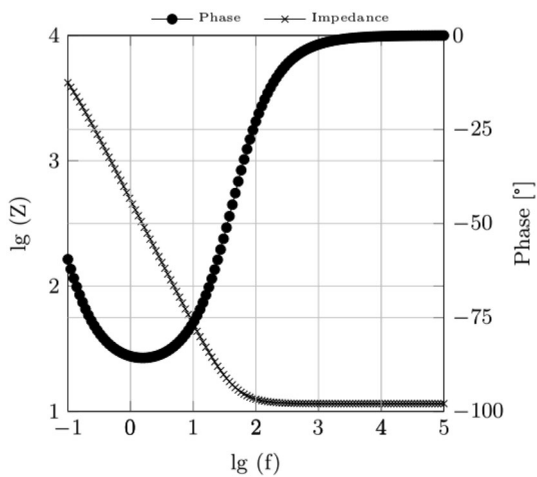
Fig. 61: Bode-plot spectra of sample 2, *t* = 24 h

Bandgap

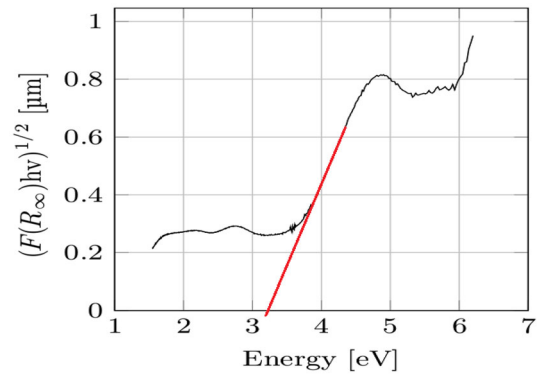See Figs. 62, 63, 64, 65, 66, 67, and 68.

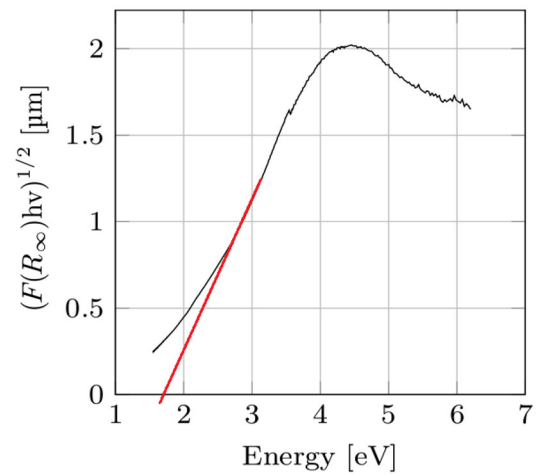**Fig. 62: Bandgap examination of sample 2**

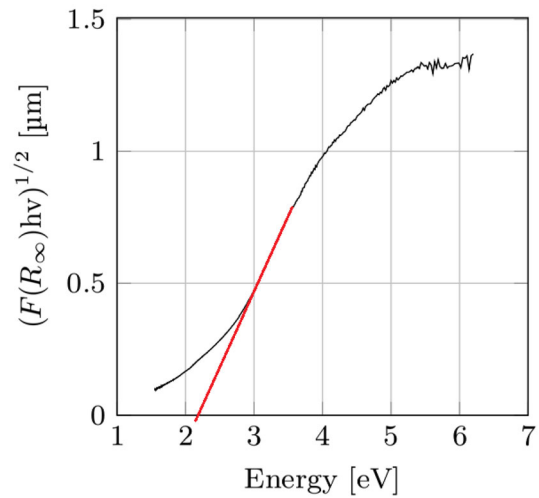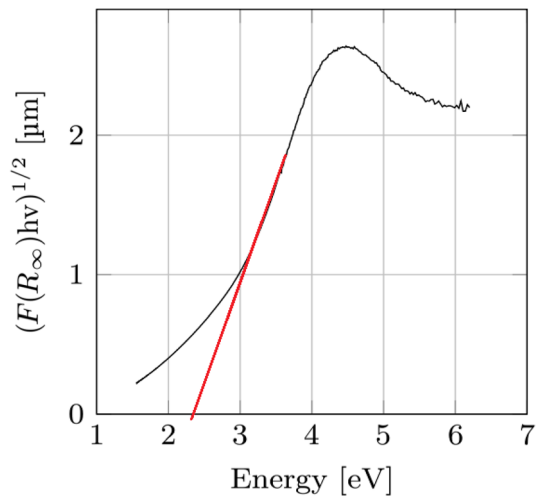**Fig. 63: Bandgap examination of sample 6**

Fig. 64: Bandgap examination of sample 7

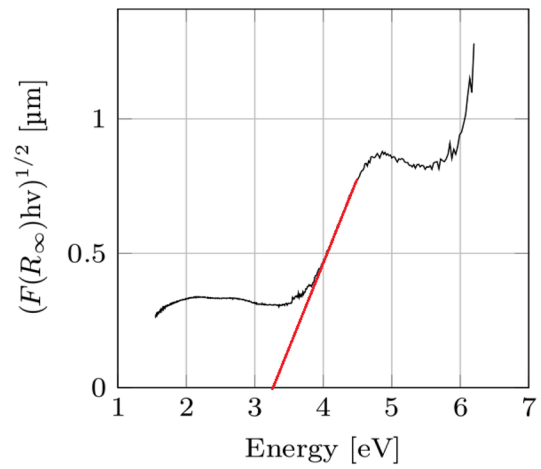**Fig. 65: Bandgap examination of sample 8**

Fig. 66: Bandgap examination of sample 2 + 6
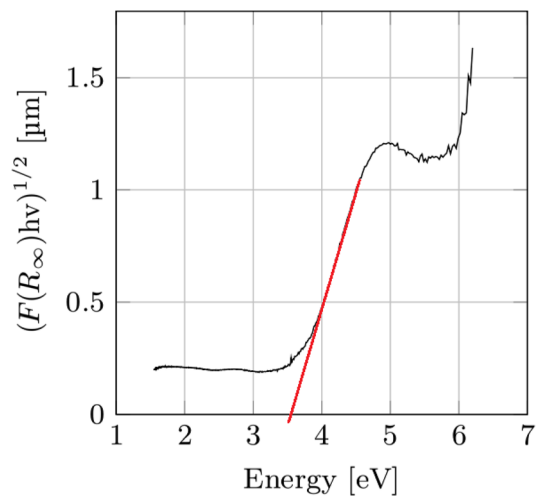

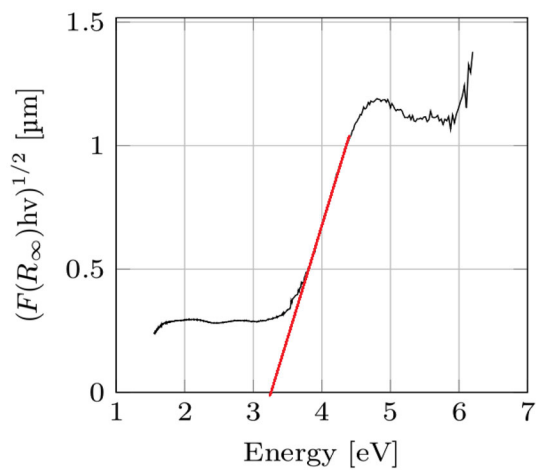**Fig. 67: Bandgap examination of sample 2 + 7**

Fig. 68: Bandgap examination of sample 2 + 8

Salt spray test

Noncoated steel

See Fig. 69.

Fig. 69: Noncoated steel after 650 h SST. Delamination: 8.9 mm, Corrosion: 0.1 mm

Sample 6

See Fig. 70.

Fig. 70: Sample 6 after 650 h SST. Delamination: Ø = 5.3 mm, Corrosion: Ø = 0.3 mm

Sample 7

See Fig. 71.

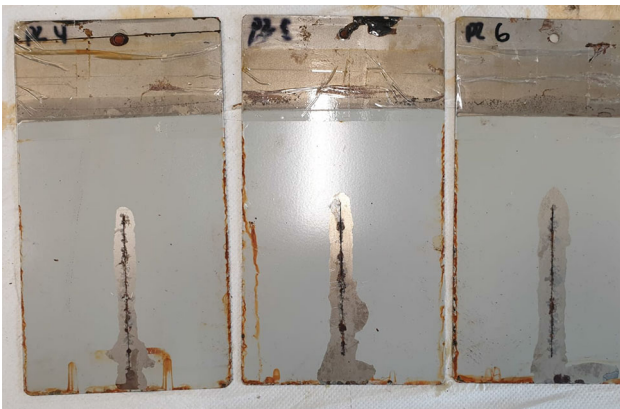**Fig. 71: Sample 7 after 650 h SST. Delamination: Ø = 6.0 mm, Corrosion: Ø = 0.3 mm**
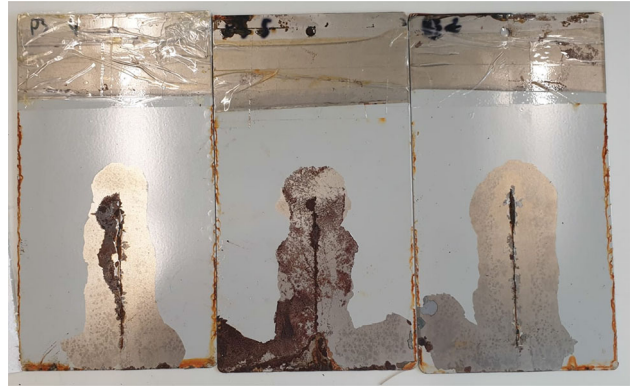
Sample 8

See Fig. 72.

Fig. 72: Sample 8 after 650 h SST. Delamination: Ø = 19.8 mm, Corrosion: Ø = 0.5 mm

Sample 2

See Fig. 73.

Fig. 73: Sample 2 after 650 h SST. Delamination: Ø = 12.2 mm, Corrosion: Ø = 0.5 mm

Sample 2 + sample 6

See Fig. 74.

Fig. 74: Sample 2 + sample 6. Delamination: Ø = 2.2 mm, Corrosion: Ø = 0.3 mm

Sample 2 + sample 7

See Fig. 75.

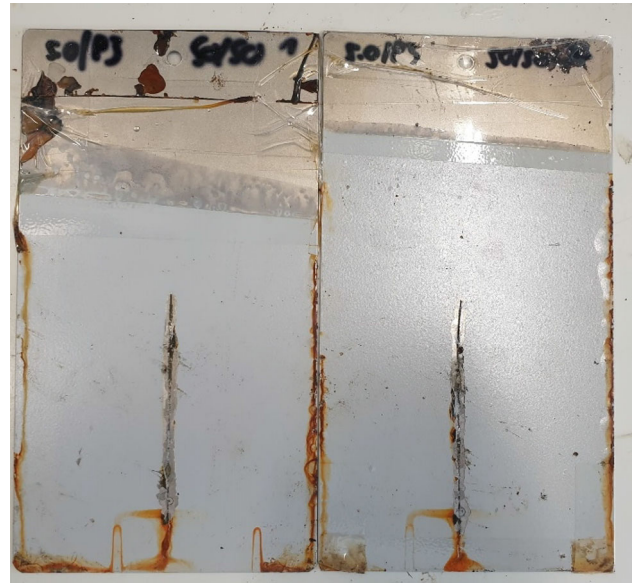**Fig. 75: Sample 2 + sample 7. Delamination: Ø = 2.1 mm, Corrosion: Ø = 0.3 mm**

Sample 2 + sample 8

See Fig. 76.

Fig. 76: Sample 2 + sample 8. Delamination: Ø = 1.7 mm, Corrosion: Ø = 0.2 mm

Other spectra

See Fig. 77.

Fig. 77: The dip bath from sample 1 (left) and sample 1 with 0.05 g iron oxide (right)

References

1. Meng, G, Sun, F, Shaoa, Y, "Effect of Phytic Acid on the Microstructure and Corrosion Resistance of Ni Coating." *Electrochim. Acta*, **55** 5990–5995 (2010)
2. Dornbusch, M, Biehler, T, Conrad, M, Greiwe, A, Momper, D, Schmidt, L, Wiedow, M, "Unusable Pretreatment of Steel and Zinc Surfaces Based on Phytic Acid." *JUnQ*, **6** (2) 1–7 (2016)
3. Yan, R, Gao, X, He, W, et al. "A Simple and Convenient Method to Fabricate New Type of Phytic Acid Metal Conversion Coatings with Excellent Anti Corrosion Perfor-

mance on the Iron Substrate." *RSC Adv.*, **7** 41152–41162 (2017)

4. Chidiebere, M, Emeka, O, Li, L, et al. "Corrosion Inhibition of Q235 Mild Steel in 0.5 M H$_2$SO$_4$ Solution by Phytic Acid and Synergistic Iodide Additives." *Ind. Eng. Chem. Res.*, **53** 7670–7679 (2014)

5. Mohammadloo, HE, Sarabi, AA, "Titanium-Phytic Acid Nano Structured Conversion Coating Formation on CRS Substrate." *Prog. Org. Coat.*, **101** 391–399 (2016)

6. Koch, GH, Brongers, MPH, Thompson, NG, Virmani, YP, Payer, JH, "Corrosion Cost and Preventive Strategies in the United State, National Technical Information Service." Report No. FHWA-RD-01-156 (2001)

7. Hesse, M, Meier, H, Zeeh, B, *Spektroskopische Methoden in der Organischen Chemie*, 7th edn. Georg Thieme Verlag, Stuttgart, p. 49 (2005)

8. Socrates, G, *Infrared and Raman Characteristic Group Frequencies: Tables and Charts*, 3rd edn. Wiley-VCH, Chichester (2018)

9. Hao, HF, Tan, HQ, Li, J, Wang, YQ, Xun, JQ, "Synergistic Effect of Cerium Conversion Coating and Phytic Acid Conversion Coating on AZ31B Magnesium Alloy." *Surf. Coat. Technol.*, **212** 32–36 (2012)

10. Pan, F, Yang, X, Zhang, D, "Chemical Nature of Phytic Acid Conversion Coating on AZ61 Magnesium Alloy." *Appl. Surf. Sci.*, **255** 8363–8371 (2009)

11. Zhang, M, Cai, S, Zhang, F, "Preparation and Corrosion Resistance of Magnesium Phytic Acid/Hydroxyapatite Composite Coatings on Biodegradable AZ31 Magnesium Alloy." *J. Mater. Sci. Mater. Med.*, **28** (82) 81–82 (2017)

12. Li, L, Zhang, G, Su, Z, "One-Step Assembly of Phytic Acid Metal Complexes for Superhydrophilic Coatings." *Angew. Chem.*, **55** (33) 9093–9096 (2016)

13. Gao, X, Lu, K, Xu, L, et al. "Excellent Anti-Corrosive Pretreatment Layer on Iron Substrate Based on Three-Dimensional Porous Phytic Acid/Silane Hybrid." *Nanoscale*, **3** 1555–1564 (2016)

14. Liu, G, Yang, L, Du, N, "Study of Molybdate-Phytic Acid Passivation on Galvanised Steel." *Corros. Eng. Sci. Technol.*, **46** (4) 542–546 (2011)

15. Gao, X, Li, W, Yan, R, et al. "Effect of Zinc Ion on the Microstructure and Electrochemical Behavior of Phytic Acid Based Conversion Coating on Q235 Steels." *Surf. Coat. Technol.*, **325** 41152–41156 (2017)

16. Sala, M, Makuc, D, Kolar, J, et al. "Potentiometric and ^{31}P NMR Studies on Inositol Phosphates and Their Interaction with Iron(III) Ions." *Carbohydr. Res.*, **346** (4) 2–9 (2011)

17. Yao, C, Xing, W, Ma, C, et al. "Synthesis of Phytic Acid-Based Monomer for UV-Cured Coating to Improve Fire Safety of PMMA." *Prog. Org. Coat.*, **140** 94–100 (2020)

18. Hull, S, Gray, J, Montogomery, R, "Autohydrolysis of Phytic Acid." *Anal. Biochem.*, **266** 16499–16505 (1999)

19. Deneluti, A, Matos, J, "Study of Thermal Behavior of Phytic Acid, Brazilian." *J. Pharm. Sci.*, **49** (2) 275–282 (2013)

20. Sakai, H, Ikemoto, Y, Kinoshita, T, et al. "Fourier-Transform Spectra of Metal Salts of Phytic Acid in the Mid- to Far-Infrared Spectral Range." *Vib. Spectrosc.*, **10** 1–11 (2017)

21. Larkin, P, *Infrared and Raman Spectroscopy: Principles and Spectral Interpretation*, 2nd edn. Elsevier, Edinburgh (2017)

22. Haansnoot, CAG, de Leeuw, FAAM, Altona, C, "The Relationship Between Proton-Proton NMR Coupling Constants and Substituent Electronegativities–I : An Empirical Generalization of the Karplus Equation." *Tetrahedron*, **36** (36) 2783–2792 (1980)

23. Coxon, B, "Developments in the Karplus Equation as they Relate to the NMR Coupling Constants of the Carbohydrates." *Adv. Carbohydr. Chem. Biochem.*, **62** 17–82 (2009)

24. Qiu, D, Guerry, P, Knowles, J, "Formation of Functional Phosphosilicate Gels from Phytic Acid and Tetraethyl Orthosilicate." *J. Sol-Gel Sci. Technol.*, **48** 378–383 (2008)

25. Isbrant, L, Oertel, R, "Conformational States of Myo-Inositol Hexakis(Phosphate) in Aqueous Solution. A Carbon-13 NMR, Phosphorus-31 NMR, and Raman Spectroscopic Investigation." *J. Am. Chem. Soc.*, **102** (9) 3144–3148 (1980)

26. Emsley, J, Niazi, S, "The Structure of Myo-Inositol Hexaphosphate Solution: ^{31}P N.M.R. Investigation." *Phosphorus Sulfur*, **10** (3) 401–408 (1981)

27. Mubarak, Y, "Production of Crystalline Urea Phosphate Using the Untreated Jordanian Wet Process Phosphoric Acid." *Eng. Sci.*, **38** 61–70 (2011)

28. Shi, H, Han, E, Liu, F, et al. "Protection of 2024–T3 Aluminum Alloy by Corrosion Resistant Phytic Acid Conversion Coating." *Appl. Surf. Sci.*, **11–235** 2–19 (2013)

29. Rausch, W, Blum, H, *Die Phosphatierung von Metallen*, vol 2, Leuze Verlag, Bad Salgau, pp. 299–304 (1998)

30. Humer, E, Schwarz, C, Schedle, K, "Phytate in Pig and Poultry Nutrition." *Anim. Physiol. Anim. Nutr.*, **99** 605–625 (2014)

31. Gupta, RK, Mensah-Darkwa, K, Sankar, J, Kumar, D, "Enhanced Corrosion Resistance of Phytic Acid Coated Magnesium by Stearic Acid Treatment." *Trans. Nonferrous Met. Soc. China*, **23** 1237–1244 (2013)

32. Vormoor, M, Dissertation: Untersuchung zur Superhydrophilie von Titandioxid-Beschichtungen, Universität Hannover, p. 25 (2009)

33. John Xavier, R, Prabaharan, A, "Vibrational Spectroscopic Investigations of 4,4-Dimethyl-2-Oxazoline: A Density Functional Theory Approach." *Spectrochim. Acta Part A Mol. Biomol. Spectrosc.*, **136** 1530–1542 (2015)

34. Dornbusch, M, *Corrosion Analysis*, CRC Press, Boca Raton, London, New York, p. 43 (2018)

35. Klusmann, E, König, U, Schultze, JW, "Elektrochemische Charakterisierung von Phosphatschichten auf Verzinktem Stahl." *Mater. Corros.*, **46** (2) 83–91 (1995)

36. Kessler, W, *Multivariate Datenanlyse für die Pharma, Bio-Prozessanalytik*, 1st edn. Wiley-VCH, Weinheim (2011)

37. Kaesche, H, *Die Korrosion der Metalle*, 3rd edn. Springer, Berlin Heidelberg, pp. 72–74 (1990)

38. Barsoukov, E, Macdonald, JR, *Impedance Spectroscopy: Theory, Experiment, and Applications*, 3rd edn. Wiley-VCH, Hoboken, p. 60 (2018)

39. Hamann, CH, Vielstich, W, *Elektrochemie*, 4th edn. Oldenburg, Wiley-VCH, p. 301 (2015)

40. Heil, TJ, Dissertation: Ersatzschatzbild-Basierte Modellierung der Diffusion und des Ladungsdurchtritts in Lithium-Ionen-Zellen, Universität München (2020)

41. Gao, HF, Tan, HQ, Li, J, "Synergistic Effect of Cerium Conversion Coating and Phytic Acid Conversion Coating on AZ31B Magnesium Alloy." *Surf. Coat. Technol.*, **212** 32–36 (2012)

42. Mohammadloo, HE, Sarabi, AA, Asemani, HR, Ahmadi, P, "A Comparative Study of Eco-Friendly Hybrid Thin Films: With and Without Organic Coating Application." *Prog. Org. Coat.*, **125** 432–442 (2018)

Publisher's Note Springer Nature remains neutral with regard to jurisdictional claims in published maps and institutional affiliations.